

# Induced scalarization in boson stars and scalar gravitational radiation

Milton Ruiz<sup>1,\*</sup>, Juan Carlos Degollado<sup>2,†</sup>, Miguel Alcubierre<sup>3,‡</sup>, Darío Núñez<sup>3,§</sup> and Marcelo Salgado<sup>3,¶</sup>

<sup>1</sup>*Departament de Física, Universitat de les Illes Balears,*

*Cra. Valldemossa Km. 7.5, Palma de Mallorca, E-07122, Spain*

<sup>2</sup>*Instituto de Astronomía, Universidad Nacional Autónoma de México,*

*Circuito Exterior C.U., A.P. 70-264, México D.F. 04510, México*

<sup>3</sup>*Instituto de Ciencias Nucleares, Universidad Nacional Autónoma de México,*

*Circuito Exterior C.U., A.P. 70-543, México D.F. 04510, México*

(Dated: July 27, 2012)

The dynamical evolution of boson stars in scalar-tensor theories of gravity is considered in the physical (Jordan) frame. We focus on the study of spontaneous and induced scalarization, for which we take as initial data configurations on the well-known S-branch of a single boson star in general relativity. We show that during the scalarization process a strong emission of scalar radiation occurs. The new stable configurations (S-branch) of a single boson star within a particular scalar-tensor theory are also presented.

PACS numbers: 04.50.-h, 04.50.Kd, 04.20.Ex, 04.25.D-, 95.30.Sf

## I. INTRODUCTION

Scalar-tensor theories (STT) are alternative theories of gravitation where a spin-0 degree of freedom  $\phi$  can accompany the usual tensor spin-2 modes (see Ref. [1] for a review). There are two mathematical representations of the STT: 1) The physical frame (also known as the “Jordan” frame), where test particles follow geodesics of spacetime and the scalar field  $\phi$  couples non-minimally to the curvature: 2) The Einstein frame, obtained by a conformal transformation of the metric, where the scalar field couples minimally to the curvature and non-minimally to the matter fields [2].

STT are perhaps the simplest, well motivated and most competitive theories of gravitation after General Relativity (GR), the most prominent example being the well-known Jordan-Brans-Dicke theory [3, 4]. Intuitively, STT can be seen as theories with a varying effective gravitational “constant”. Although so far there is not observational evidence that such scalar gravitational field exists, one can use the experimental and observational tests of GR to put limits on its existence and its possible interactions [5]. Using data from the binary pulsar, for instance, it is possible to put limits on some classes of STT which restrict the form of the non-minimal coupling (NMC) to the curvature. Nevertheless, these bounds still allow a NMC constant of order unity [6].

Despite the fact that STT were proposed several decades ago, it has only been recently that several phenomena associated with them, and with no counterpart in GR, have been analyzed. For instance, in the cosmological context, STT have been proposed as alternatives

to the cosmological constant in order to explain the accelerated expansion of the Universe [7–12].

In the astrophysical scenario, Damour and Esposito-Farèse [6, 13] discovered that neutron star models within STT may undergo a *phase transition* that consists on the appearance of a non-trivial configuration of the scalar field  $\phi$  in the absence of sources and with vanishing asymptotic value. This phenomenon has been named *spontaneous scalarization* (SS) due to its similarities with the spontaneous magnetization of ferromagnets at low temperatures. The stability analysis for the transition to SS was first performed by Harada [14, 15]. It is now understood that SS arises under certain conditions where the appearance of a non-trivial scalar field gives rise to a stationary configuration that minimizes the energy of the star with fixed baryon number.

Further analysis have confirmed that the SS phenomenon takes place in neutron stars independently of the equation of state (EOS) used to describe the nuclear matter [16–18]. In boson stars this phenomenon was first studied by Whinnett [19], who constructed stationary scalarized configurations with a self-interaction potential for the scalar field. More recently, the dynamic transition to SS was analyzed by us in the Jordan frame and without self-interaction [20]. One important feature of this phenomenon is that it can occur even when the parameters of the theory satisfy the stringent bounds imposed by the Solar System experiments, notably, when the Brans-Dicke parameter is chosen to be arbitrarily large.

The SS phenomenon is accompanied by the “sudden” appearance of a new global quantity termed *scalar charge*, where by sudden we mean that the derivative of this charge with respect to the central energy density at the critical point is infinite. The scalar charge is the analogous of the magnetization of ferromagnets mentioned above. Moreover, just as in the neutron star case, in boson stars one also finds that beyond a certain critical central energy-density, the stationary configurations that are energetically preferred are those where the SS

\*Electronic address: milton.ruiz@uib.es

†Electronic address: jdaza@astro.unam.mx

‡Electronic address: malcubi@nucleares.unam.mx

§Electronic address: nunez@nucleares.unam.mx

¶Electronic address: marcelo@nucleares.unam.mx

ensues.

A phenomenon similar to SS, but that occurs when a background scalar field is present, is called *induced scalarization* (IS). It corresponds to the case where the scalar field does not vanish asymptotically. In this situation the scalar charge does not exhibit a discontinuous “jump” as the object becomes more compact, and the transition to scalarization is smoothed out by the presence of the background field.

Another important feature of STT is the prediction of scalar gravitational waves. While GR predicts only quadrupole gravitational radiation in the “far zone”, STT predicts the existence of monopolar gravitational waves that can be emitted even in the case of spherical symmetry [21]. The new polarization of this scalar mode is of *breathing type* since it affects all directions isotropically [21].

A simple scenario where such scalar gravitational waves might be produced is precisely during the scalarization process of a spherical compact object. The amplitude of such waves (in the linear approximation) is linked directly with both the form of the NMC and the asymptotic value of the scalar field. For instance, when this asymptotic value vanishes, it turns out that certain classes of STT do not lead to the emission of scalar gravitational waves. This implies in particular that in such classes of STT the SS phenomenon does not produce monopolar waves, rather it is only in the IS scenario that such theories can lead to an emission of scalar gravitational radiation. Since we will be working with one such class of STT, it is then particularly important to make a clear distinction between the SS and the IS phenomena.

The first dynamical analysis of the scalarization phenomenon in neutron stars was made by Novak [16]. He did not only confirm the dynamical transition to the scalarization state, but also the emission of scalar gravitational waves. Moreover, he also studied the emission of scalar gravitational radiation when a scalarized star collapses into a black hole [22].

Recent studies of neutron star oscillations within STT have shown that, in addition to the emission of scalar gravitational waves, the quadrupole gravitational radiation is also disturbed as compared to the corresponding signals in GR [23]. Therefore, even if the detection channels for scalar gravitational waves are “switched off”, the detection of gravitational waves of spin-2 coming from these sources might still validate STT or put even more stringent bounds on their parameters. Of course, the direct detection of scalar gravitational waves (or the absence thereof) would also help to discriminate between several alternative theories.

In this work, we present a systematic study of the phenomenon of IS in the spacetime of a single boson star, without a self-interaction potential for the non-minimally coupled scalar field. We choose to work directly in the physical Jordan frame where the physics is better understood. In addition, we study some properties of the gravitational scalar waves such as their magnitude and

frequency. All the numerical evolutions are performed in spherical symmetry using a 3+1 formalism of STT as presented in [24]. However, instead of evolving the geometry with the Arnowitt-Deser-Misner (ADM) equations, we use a strongly hyperbolic version similar to the Baumgarte-Shapiro-Shibata-Nakamura (BSSN) formulation [25, 26] but adapted to the STT [27]. Using this 3+1 system the initial value problem of STT in the Jordan frame turns to be well-posed. Nevertheless, at the moment we only have numerical evidence to show that the initial *boundary* value problem (IBVP) is also well-posed. The analysis of the continuum IBVP for this system will be presented elsewhere.

This paper is organized as follows. Section II introduces the STT and discusses briefly some properties associated with the Jordan frame. The relevant 3+1 equations of [24] are also presented. For completeness, and for the benefit of the reader, in Section III we discuss the heuristic analysis performed by Damour and Esposito-Farèse in [13], which allows one to understand the scalarization phenomenon on simple grounds. Section IV contains our boson star model. In Section V we describe the scalar waves predicted in STT. Section VI summarizes the setup used in the numerical code. We present the results of our numerical simulation in Section VII, and we conclude in Section VIII.

We also present in Appendix A the characteristic decomposition of the spherically symmetric equations used in this paper, which allow us to conclude that our system is strongly hyperbolic and, therefore, that the Cauchy problem is well-posed for the spherically symmetric case. In Appendix B we present some numerical evidence that indicates that corresponding IBVP is also well-posed.

## II. SCALAR TENSOR THEORIES OF GRAVITY

### A. Field equations

The STT of gravitation are one of the simplest and most analyzed alternative theories of gravity. These alternative theories were introduced by Jordan during the decade of the fifties [3], and then reanalyzed by Brans and Dicke later [4]. The general action for STT in the Jordan frame, where gravity is coupled non-minimally to a single scalar field  $\phi$ , is given by

$$S[g_{ab}, \phi, \psi] = \int \left\{ \frac{F(\phi)}{16\pi G_0} R - \frac{1}{2} (\nabla\phi)^2 - V(\phi) \right\} \sqrt{-g} d^4x + S_{\text{matt}}[g_{ab}, \psi], \quad (2.1)$$

where  $\psi$  represents all the matter fields, *i.e.* fields other than  $\phi$ ,  $G_0$  is the usual gravitational constant,  $F(\phi)$  is some NMC function to be specified later, and  $V(\phi)$  represents a potential for  $\phi$  (we use units such that  $c = 1$ ). In fact, in all the numerical analysis considered here, we will not consider the potential  $V(\phi)$ . However, for completeness it will be included in the field equations displayed

below. Notice that one can identify the “effective” gravitational constant as the coefficient  $G_{\text{eff}}(\phi) = G_0/F(\phi)$  that appears in the above action [63].

From the above action, one finds the following field equations:

$$R_{ab} - \frac{1}{2}g_{ab}R = 8\pi G_0 T_{ab}, \quad (2.2)$$

$$\square\phi + \frac{1}{2}f'R = V', \quad (2.3)$$

where a prime indicates  $\partial_\phi$ ,  $\square := g^{ab}\nabla_a\nabla_b$  is the standard covariant d’Alambertian operator, and

$$T_{ab} := \frac{G_{\text{eff}}}{G_0} \left( T_{ab}^f + T_{ab}^\phi + T_{ab}^{\text{matt}} \right), \quad (2.4)$$

$$T_{ab}^f := \nabla_a (f' \nabla_b \phi) - g_{ab} \nabla_c (f' \nabla^c \phi), \quad (2.5)$$

$$T_{ab}^\phi := (\nabla_a \phi)(\nabla_b \phi) - g_{ab} \left[ \frac{1}{2}(\nabla \phi)^2 + V(\phi) \right], \quad (2.6)$$

with  $T_{ab}^{\text{matt}}$  the stress-energy tensor of all matter fields other than  $\phi$ , and where we have defined

$$f := \frac{F}{8\pi G_0}, \quad G_{\text{eff}} := \frac{1}{8\pi f}. \quad (2.7)$$

Notice that equation (2.2) implies that the Ricci scalar can be expressed in terms of the trace of the energy-momentum tensor (2.4). Therefore, Eq. (2.3) can be rewritten in the form

$$\square\phi = \frac{2fV' - 4f'V - f'(1+3f'')(\nabla\phi)^2 + f'T_{\text{matt}}}{2f(1+3f'^2/2f)}, \quad (2.8)$$

with  $T_{\text{matt}}$  the trace of  $T_{ab}^{\text{matt}}$ . On the other hand, the Bianchi identities directly imply

$$\nabla_c T^{ca} = 0. \quad (2.9)$$

Nevertheless, the use of the field equations leads to the conservation of the energy-momentum tensor of the matter alone

$$\nabla_c T_{\text{matt}}^{ca} = 0, \quad (2.10)$$

which implies the fulfillment of the (weak) equivalence principle, *i.e.* test particles follow geodesics of the metric  $g_{ab}$ .

## B. 3+1 decomposition

In order to recast the previous field equations as a Cauchy initial value problem [28, 29], we first rewrite the four-dimensional metric in 3+1 form as

$$ds^2 = -(\alpha^2 - \beta^i \beta_i) dt^2 + 2\beta_i dx^i dt + \gamma_{ij} dx^i dx^j, \quad (2.11)$$

with  $\alpha$  the lapse function,  $\beta^i$  the shift vector, and  $\gamma_{ij}$  the 3-metric induced on the spatial hypersurfaces.

We perform a 3 + 1 decomposition of equations (2.2) and (2.3), using the normal timelike vector  $n^a$  to the spacelike hypersurfaces  $\Sigma_t$ , and the projection operator  $P^a_b = \delta^a_b + n^a n_b$ . In order to do so, we first define the first order variables:

$$Q_i := D_i \phi = P_i^k \nabla_k \phi, \quad (2.12)$$

$$\Pi := n^a \nabla_a \phi = \frac{1}{\alpha} \frac{d\phi}{dt}, \quad (2.13)$$

where  $D_i$  is the covariant derivative compatible with the 3-metric  $\gamma_{ij}$ , and  $d/dt := \partial_t - \mathcal{L}_\beta$ , with  $\mathcal{L}_\beta$  the Lie derivative along the shift vector. Notice that the relevant components of the quantities computed with  $P^a_b$  are the spatial ones. It is now straightforward to show that  $Q_i$  and  $\Pi$  evolve according to [24],

$$\frac{dQ_i}{dt} = D_i(\alpha \Pi), \quad (2.14)$$

$$\begin{aligned} \frac{d\Pi}{dt} = & \alpha [\Pi K + Q^l D_l(\ln \alpha) + D_l Q^l] \\ & - \frac{\alpha}{2f \left(1 + \frac{3f'^2}{2f}\right)} \left[ 2fV' - 4f'V \right. \\ & \left. - f'(1+3f'')(Q^2 - \Pi^2) + f'T_{\text{matt}} \right]. \end{aligned} \quad (2.15)$$

We define the energy density  $\rho := n^a n^b T_{ab}$ , momentum density  $J_a := -P^b_a n^c T_{bc}$  and a stress tensor  $S_{ab} := P^c_a P^d_b T_{cd}$ . From (2.4) we find

$$\rho = \frac{G_{\text{eff}}}{G_0} (\rho^f + \rho^\phi + \rho^{\text{matt}}), \quad (2.16)$$

$$J_i = \frac{G_{\text{eff}}}{G_0} (J_i^f + J_i^\phi + J_i^{\text{matt}}), \quad (2.17)$$

$$S_{ij} = \frac{G_{\text{eff}}}{G_0} (S_{ij}^f + S_{ij}^\phi + S_{ij}^{\text{matt}}). \quad (2.18)$$

Using now Eqs. (2.7) and (2.8), one can show that [24]

$$\begin{aligned} \rho = & \frac{1}{8\pi G_0 f} \left[ f' (D_k Q^k + K \Pi) + \frac{\Pi^2}{2} \right. \\ & \left. + \frac{Q^2}{2} (1 + 2f'') + V(\phi) + \rho_{\text{matt}} \right], \end{aligned} \quad (2.19)$$

$$\begin{aligned} J_i = & \frac{1}{8\pi G_0 f} \left[ -f' (K_i^k Q_k + D_i \Pi) \right. \\ & \left. - \Pi Q_i (1 + f'') + J_i^{\text{matt}} \right], \end{aligned} \quad (2.20)$$

$$\begin{aligned} S_{ij} = & \frac{1}{8\pi G_0 f} \left\{ Q_i Q_j (1 + f'') + f' (D_i Q_j + \Pi K_{ij}) \right. \\ & + \frac{\gamma_{ij}}{\left(1 + \frac{3f'^2}{2f}\right)} \left[ \frac{1}{2} (Q^2 - \Pi^2) \left( 1 + \frac{f'^2}{2f} + 2f'' \right) \right. \\ & \left. + V \left( 1 - \frac{f'^2}{2f} \right) + f'V' + \frac{f'^2}{2f} (S_{\text{matt}} - \rho_{\text{matt}}) \right] \\ & \left. + S_{ij}^{\text{matt}} \right\}. \end{aligned} \quad (2.21)$$

where we have defined  $Q^2 := Q^l Q_l$ .

Notice that the 3 + 1 decomposition of (2.2) are just the usual ADM equations given by

$$\frac{d\gamma_{ij}}{dt} = -2\alpha K_{ij}, \quad (2.22)$$

$$\begin{aligned} \frac{dK_{ij}}{dt} = & -\nabla_i \nabla_j \alpha + \alpha [R_{ij} + K K_{ij} - 2K_{il} K^l_j] \\ & + 4\pi G_0 \alpha [\gamma_{ij} (S - \rho) - 2S_{ij}], \end{aligned} \quad (2.23)$$

where  $R_{ij}$  is the 3-dimensional Ricci tensor associated with the spatial metric  $\gamma_{ij}$ , and the effective matter terms are given by Eqs. (2.19)–(2.21). The Hamiltonian and momentum constraints take the form

$$H := \frac{1}{2} (R + K^2 - K_{ij} K^{ij}) - 8\pi G_0 \rho = 0, \quad (2.24)$$

$$M^i := D_l (K^{il} - \gamma^{il} K) - 8\pi G_0 J^i = 0. \quad (2.25)$$

Formally, one should also consider the constraint  $D_{[i} Q_{j]} = 0$ , which corresponds to the integrability condition  $\partial_{ij}^2 \phi = \partial_{ji}^2 \phi$ . The above system of evolution equations has to be completed with appropriate evolution equations for the gauge variables. This issue is considered below.

### C. Gauge choice

To obtain a closed evolution system, one has to impose gauge conditions for the time variable  $t$  and for the spatial coordinates  $x^i$ . Following [27], we will consider a modified Bona-Masso (MBM) time slicing condition [30]. In local coordinates adapted to the 3 + 1 foliation  $x^a = (t, x^i)$ , this slicing condition is given by

$$\frac{d\alpha}{dt} = -\alpha^2 f_{BM}(\alpha) \left[ K - \frac{\Theta}{f_{BM}(\alpha)} \frac{f'}{f} \Pi \right], \quad (2.26)$$

with  $f_{BM}(\alpha) > 0$  the usual Bona-Masso gauge function and  $\Theta$  a free parameter.

The specific choices  $\Theta = f_{BM} = 1$  correspond to a modified harmonic slicing condition (termed “pseudo-harmonic” in [24, 27]), which was specially useful for the second order hyperbolicity analysis performed in [24]. On the other hand, with  $\Theta = 0$  one recovers the usual Bona-Masso (BM) slicing condition. However, it has been shown that taking  $\Theta = 0$  does not result in a strongly hyperbolic formulation of STT in the Jordan frame [27]. For this reason, in all the simulations presented here we have used the pseudo-harmonic slice with  $\Theta = 1$ .

Concerning the propagation of the spatial coordinates, we will consider the shift vector as an *a priori* known function of the coordinates. In particular, in all our evolutions it is set to zero. However, in the future, it would be interesting to investigate some “live” shift conditions and their effects in phenomena involving STT.

## III. SCALARIZATION

The STT of gravity induce strong field effects which, for instance, produce important deviations from GR in stellar models. As mentioned before, one such effect is the SS phenomenon which is similar to the spontaneous magnetization in ferromagnetic materials at low temperatures. In the following, we will use this analogy in order to understand the SS phenomenon.

When a ferromagnet is exposed to an external magnetic field, the individual spins of its constituents align with the field, giving rise to a permanent magnetization which remains even after the external field is switched off. Moreover, the ferromagnets have the property that, below the Curie temperature, a magnetization appears “spontaneously” even in the absence of an external magnetic field. In the STT, on the other hand, a nontrivial configuration of a scalar field may spontaneously appear during the evolution of a compact object in the absence of external sources, *i.e.* without a potential  $V(\phi)$ . One can then identify the external magnetic field with a background (cosmological) scalar field and the temperature with the inverse of the central energy-density  $\rho_c^{\text{matt}}$  of the matter content or, equivalently, with the inverse of total baryon mass (in the case of neutron stars). The roll of the magnetization is played by a new global quantity called the *scalar charge*  $Q_{\text{scal}}$ , which will be defined below and which corresponds to the coefficient of  $\phi(r) \sim Q_{\text{scal}}/r$  in the asymptotic region. This means that beyond a certain critical density or critical baryon mass, the transition to the spontaneous scalarization ensues. In this case  $\partial Q_{\text{scal}}/\partial \rho_c^{\text{matt}}$  is infinite at the critical energy-density. This transition can be smoothed by the presence of a non-zero background scalar field  $\phi_0$ .

In practice, when the phenomenon is analyzed in static configurations, the value  $\phi_0$  is usually fixed by a shooting method [18, 31]. It is important to emphasize the relevance of not adding sources to the scalar field equation. Indeed, a non-zero potential can make the scalar field decrease so fast that the scalar charge might in fact vanish at infinity.

An interesting analytical toy model to understand this phenomenon is the following [6]. Consider a static and spherically symmetric compact object represented by an incompressible fluid (constant energy-density), whose profile density is given by a step function. Moreover, assume that the function  $F(\phi)$  in the action for STT is just a quadratic function of,  $F(\phi) = 1 + 8\pi G_0 \xi \phi^2$ , and the potential  $V(\phi)$  vanishes. Finally, assume  $R \approx -8\pi G_0 T_{\text{matt}} \approx 8\pi G_0 \rho_{\text{matt}}$  (as in GR). This implies, for instance, that the generalized Klein-Gordon Eq. (2.3) is linear in  $\phi$ . Furthermore, by neglecting all the gravitational effects in this equation, one ends-up with a Helmholtz-like equation of the form  $\Delta\phi + k^2\phi = 0$ , where the mass-like term  $k^2 = 8\pi G_0 \xi \rho_{\text{matt}}$  depends on both the constant energy-density of the matter and the NMC constant  $\xi$ . Notice that in this simplified model, the mass term vanishes beyond the surface of the compact object.



Now, for  $\xi > 0$  the interior regular spherically symmetric solution of the above Helmholtz equation is given by

$$\phi_{\text{int}}(r) = \phi_c \frac{\sin(kr)}{kr}, \quad (3.1)$$

where  $\phi_c$  is the scalar field at the origin  $r = 0$ . The exterior solution is

$$\phi_{\text{ext}}(r) = \frac{C}{r} + \phi_0, \quad (3.2)$$

where  $C$  is an integration constant and  $\phi_0$  is the asymptotic value of the scalar field.

When both solutions are matched continuously at the surface of the object  $r = \mathcal{R}$  [ $\rho_{\text{matt}}(r \geq \mathcal{R}) = 0$ ], it turns out that  $\phi_c = \phi_0 / \cos(k\mathcal{R})$ . The explicit form for the constant  $C$  is not relevant for the analysis (but one finds  $C \propto \phi_c \mathcal{R}$ ). Note that if  $\phi_0 = 0$ , automatically  $\phi_c = 0 = C$  and, therefore,  $\phi(r) \equiv 0$ . In this case, there is no scalarization. On the other hand, a different situation can happen if  $\cos(k\mathcal{R})$  vanishes as well when  $\phi_0 \rightarrow 0$ . This can occur when  $k = \pi/(2\mathcal{R})$ . In this case, the solution is given by

$$\phi_{\text{int}}(r) = \frac{\epsilon \sin(\bar{r})}{\bar{r}}, \quad (3.3)$$

$$\phi_{\text{ext}}(r) = \frac{\epsilon}{\bar{r}}, \quad (3.4)$$

where  $\epsilon$  is a constant related to the scalar charge  $Q_{\text{scal}}$  whose numerical value depends on the details of the model, and  $\bar{r} = r\pi/(2\mathcal{R})$ . The above simplified analysis agrees qualitatively with the full numerical study [6, 16, 18]. Note that if  $\xi < 0$ , the interior solution is  $\phi_{\text{int}}(r) = \phi_c \sinh(|k|r)/(|k|r)$  and  $\phi_c = \phi_0 / \cosh(|k|\mathcal{R})$ . In this case, the scenario is completely different since the function  $\cosh(|k|\mathcal{R})$  never vanishes, and so when  $\phi_0 \rightarrow 0$  then automatically  $\phi_c \rightarrow 0$  and then the scalar field vanishes everywhere (no scalarization ensues). It is somehow remarkable that the spontaneous scalarization phenomenon is associated with a decreasing effective gravitational constant (*i.e.*  $G_{\text{eff}} < G_0$ ) [18].

Another way to understand the existence of these kind of scalarized configurations is to notice that the presence of a non-trivial scalar field  $\phi(r)$  (within a class of STT) causes the total energy of the stationary configuration to decrease relative to the case where  $\phi(r) = 0$  for a fixed baryon mass [13, 18]. This can also be understood on Newtonian grounds by a suitably redefinition of the kind of energy that has to be minimized when dealing with a theory where an effective gravitational “constant” may vary [18]. The energetic analysis shows that for large compactness, the energetically preferred stationary configurations are those with a non-trivial scalar field. Again, in the ferromagnetic analogy, one appreciates that in the Landau ansatz, the free energy of the ferromagnet becomes lower in the presence of magnetization than the energy in the absence of it when the temperature is below the Curie point. This occurs since below that temperature the free energy develops a global minimum and a

local maximum (like a Mexican hat potential). The local maximum of the free energy is located at zero magnetization while the minimum corresponds to a non-zero magnetization. Recently, it was also been argued that the SS phenomenon can be traced back to the quantum fluctuations of the vacuum state associated with the scalar field [32, 33].

The scalar charge which characterizes the scalarized configuration is defined as

$$Q_{\text{scal}} := - \lim_{r \rightarrow \infty} \frac{1}{4\pi\sqrt{G_0}} \int_S s_a \nabla^a \phi \, ds, \quad (3.5)$$

where  $s^a$  is the unit outward normal to a topological 2-sphere  $S$  embedded in  $\Sigma_t$ , and  $r$  is a radial coordinate that provides the area of  $S$  asymptotically. As it was remarked in the introduction, when the asymptotic value of the scalar field,  $\phi_0$ , is not demanded to vanish but is only accommodated to satisfy the Solar System bounds, then the scalarization process is *induced* by such background (cosmological) field. In such situation the transition from a small scalar charge to a large one (which depends on the compactness of the object) is smoothed out and the derivative  $\partial Q_{\text{scal}} / \partial \rho_0^{\text{matt}}$  is always finite. In this paper, we will be concerned with this latter situation only, but as long as  $\phi_0$  is small, the difference between the two type of scalarizations is just a matter of principle. Nevertheless, the important point for making such a distinction is that while in the SS case there are no emission of scalar gravitational waves (when  $F'(\phi)_{\phi_0=0} = 0$ , which is the case for the quadratic function  $F(\phi)$  considered above), for the *induced* case where  $\phi_0 \neq 0$ , one can have a small but non-zero amplitude for the scalar waves (*c.f.* Sec. V).

Another important qualitative mathematical aspect that distinguish both types of scalarizations for a NMC like the quadratic one is the following. If one considers Eq. (2.3) in absence of a potential, it turns out that  $\phi = 0$  is always a stationary solution of the equation. This implies then that  $\phi_0 \equiv 0$ . Therefore, in order to trigger the transition to a SS case an explicit scalar-field perturbation is required. An analysis of this sort was performed by us in [20]. However, if one considers initially a trivial (but non-zero) scalar-field configuration  $\phi = \phi_0 = \text{const.}$ , then this is not a stationary solution of Eq. (2.3). In such a case *a fortiori* the scalar field will evolve in time without the need of any perturbation. How much of the initial energy of the star will then be transformed into scalar energy and scalar radiation leaving behind a highly non trivial stationary scalar field configuration will depend precisely on the compactness of the object. Higher compact objects will radiate more energy in the form of scalar radiation than lower compact ones. Therefore, higher compact objects are expected to end up in a stationary scalarized state with energy lower than the initial one, the difference being radiated away in scalar-field form. Clearly, in order to analyze in detail the transition towards a scalarized state from a state with a trivial (non-zero) scalar field and its corresponding emission of scalar radiation, a dynamical evolution is

required. This is the aim of this paper.

#### IV. BOSON STARS

Boson stars are equilibrium configurations of a self-gravitating (condensate) complex scalar field. Their “hydrostatic” equilibrium is maintained by the intrinsic effective pressure of the boson field due to the uncertainty principle (for a review see Ref. [34, 35]), rather than the Pauli exclusion principle that acts, for instance, in neutron stars. Classically, one can interpret the equilibrium as a consequence of an effective pressure associated with the boson field which depends on its gradients and potential. Since the energy-density and pressure are parameterized in a certain way by the boson field itself, the relation between them provides a non-trivial EOS for this kind of matter.

Boson stars are also interpreted as macroscopic boson quantum states whose associated physical particles are formed by the excitations around the vacuum expectation value of the scalar field. The theoretical existence of such objects were proven first by Kaup [36], and later by Ruffini and Bonazzola [37], for the ground state solutions of a free boson field. Using the uncertainty principle and the definition of the Schwarzschild radius, it can be shown that the boson stars considered there have an effective radius  $R_{eff} \sim \hbar/m_b c$  and a maximum mass of

$$M_{max} \sim \frac{\hbar c}{2 G_0 m_b} = 0.5 M_{Pl}^2/m_b, \quad (4.1)$$

where  $M_{Pl}$  is the Planck mass and  $m_b$  is the mass associated with bosons (for clarity we have restored the speed of light  $c$ ). Numerical results show that, in fact, this limit is  $M_{max} \approx (2/\pi) M_{Pl}^2/m_b$ . Therefore, the resulting sizes and masses of boson stars would be so small as to be astrophysically inconsequential. In a more recent paper [38], it was shown that a self-interacting boson field (with an interaction of the form  $\sim \lambda \phi^4$ ) can give rise to stable boson stars with

$$M_{max} \sim \lambda^{1/2} M_{Pl}^2/m_b \sim \text{GeV}^2 \lambda^{1/2} M_\odot/m_b^2, \quad (4.2)$$

which is comparable with the Chandrasekhar mass for fermion stars [39]. This result was then extended to the so-called soliton stars [40, 41].

Boson star models have been constructed in the past within the framework of STT (see *e.g.* [19, 20, 42–46] and references therein), although only Whinnett had shown that the phenomenon of spontaneous scalarization occurs in these objects with the inclusion of a quartic self-interaction potential [19]. Recently, we have found that self-interactions are not in fact necessary in order to produce scalarization [20]. On the other hand, Torres has shown in [42] that, for parameters and boundary conditions respecting the weak-field limits and the nucleosynthesis bounds, the masses of boson stars in the

STT framework are comparable with the ones in GR (for stars in the ground state). Comer [43] confirmed the same trend for the case of boson stars in “excited” states. Equilibrium and stability properties for these stars in STT for different cosmic ages have been analyzed in [44, 45].

An important aspect of analyzing boson stars in the framework of STT is that the transition to a scalarized state might be accompanied by the emission of (spin-0) scalar gravitational waves (like in neutron stars). It is possible that such kind of waves might be detected in the future if fundamental scalar fields do exist in nature [21].

##### A. The Model

Boson stars are described by the Lagrangian density of a complex scalar field

$$\mathcal{L}_{\text{matt}} = -\frac{1}{2} g^{ab} \nabla_a \psi \nabla_b \psi^* - V_\psi(|\psi|^2), \quad (4.3)$$

where  $\psi$  is the scalar field,  $\psi^*$  its complex conjugate,  $|\psi|^2 = \psi \psi^*$ , and  $V_\psi(|\psi|^2)$  is a potential depending just on the norm. Variation of the above Lagrangian with respect to  $\psi$  leads to the KG equation

$$\square \psi = 2 \psi \frac{dV_\psi}{d|\psi|^2}. \quad (4.4)$$

It is straightforward to show that if the scalar field  $\psi$  is real, the KG equation (4.4) takes the usual form  $\square \psi = \partial_\psi V_\psi$ . On the other hand, variation of (4.3) with respect to the metric  $g_{ab}$  leads to the energy-momentum tensor

$$T_{ab}^{\text{matt}} = \frac{1}{2} \left[ (\nabla_a \psi^*) (\nabla_b \psi) + (\nabla_b \psi^*) (\nabla_a \psi) \right] - g_{ab} \left[ \frac{1}{2} |\nabla \psi|^2 + V_\psi(|\psi|^2) \right]. \quad (4.5)$$

We will consider only the free field case where the potential is given by

$$V_\psi(|\psi|^2) = \frac{1}{2} m^2 \psi^* \psi, \quad (4.6)$$

with  $m$  a parameter that can be considered as the “bare mass” of the theory (although it has units of inverse length). It is possible to include more general terms in (4.6), such as  $\lambda |\psi|^4$  which corresponds to a self-interaction term [38].

The Lagrangian (4.3) is invariant with respect to a global phase transformation  $\psi \rightarrow e^{iq} \psi$  (with  $q$  a real constant). The Noether theorem then implies the local conservation of the boson number  $\nabla_a \mathcal{J}^a = 0$ , where the number-density current is given by

$$\mathcal{J}^a = \frac{i}{2} g^{ab} [\psi \nabla_b \psi^* - \psi^* \nabla_b \psi]. \quad (4.7)$$

This means that the total boson number,

$$\mathcal{N} = - \int_{\Sigma_t} \sqrt{\gamma} n_a \mathcal{J}^a d^3x, \quad (4.8)$$

is conserved (here  $\gamma$  is the determinant of the 3-metric  $\gamma_{ij}$ ). The total boson mass can be defined by

$$M_{\text{bos}} := m_b \mathcal{N}, \quad (4.9)$$

where  $m_b := 2\pi \hbar m/c$  is the mass of single bosons (again we have restored the speed of light  $c$ ).

A 3+1 decomposition of the above energy-momentum tensor gives rise to the following matter variables

$$\rho_{\text{matt}} = \frac{1}{2} (|\Pi_\psi|^2 + |Q_\psi|^2) + V_\psi(|\psi|^2), \quad (4.10)$$

$$S_{\text{matt}}^{ij} = \frac{1}{2} \left( Q_\psi^{*i} Q_\psi^j + Q_\psi^{*j} Q_\psi^i \right) - \gamma^{ij} \left[ \frac{1}{2} (|Q_\psi|^2 - |\Pi_\psi|^2) + V_\psi(|\psi|^2) \right], \quad (4.11)$$

$$J_i^{\text{matt}} = -\frac{1}{2} \left( \Pi_\psi Q_i^{*\psi} + \Pi_\psi^* Q_i^\psi \right), \quad (4.12)$$

where we have defined, in analogy with (2.12) and (2.13), the variables

$$Q_i^\psi := D_i \psi, \quad (4.13)$$

$$\Pi^\psi := \frac{1}{\alpha} \frac{d\psi}{dt} = \frac{1}{\alpha} \left( \partial_t \psi - \beta^l Q_l^\psi \right). \quad (4.14)$$

According to this, one can rewrite the KG equation (4.4) as a first order PDE system like (2.14-2.15).

Before finishing this Section we must emphasize the fact that boson stars in STT involve two distinct scalar-fields, the real-valued non-minimally coupled field  $\phi$ , and the a complex-valued boson field  $\psi$ .

## V. SCALAR GRAVITATIONAL WAVES

In this section we will show that the presence of the scalar field  $\phi$  can induce the propagation of scalar (monopolar) gravitational waves. Similar analysis have been presented before in [47, 48]. Using the weak-field approximation, Wagoner has analyzed the properties of the source and its radiation in the Einstein frame [47]. On the other hand, Harada *et al.* have analyzed, in the Brans-Dicke theory, the emission of the scalar gravitational radiation in spherical dust collapse [48]. Moreover from the detection point of view, a detailed study has been performed in [21].

Let us start by considering a linear perturbation of a flat background metric  $\eta_{ab}$  and a background scalar field  $\phi_0$  such that

$$g_{ab} \approx \eta_{ab} + \epsilon \gamma_{ab}, \quad (5.1)$$

$$\phi \approx \phi_0 + \epsilon \tilde{\phi}, \quad (5.2)$$

where  $\epsilon \ll 1$  (do not confuse this  $\epsilon$  with the one in Eqs. (3.3) and (3.4)). Thus, according to the above approximation, we have

$$T_{ab} \approx \epsilon \tilde{T}_{ab}, \quad (5.3)$$

$$F(\phi) \approx F_0 + \epsilon \tilde{\phi} F'_0, \quad (5.4)$$

where the subindex 0 indicates quantities at zero order. Notice that one must in fact have  $T_0^{ab} = 0$  in order to be consistent with first order perturbations of a flat background [49].

In the generalized Lorentz gauge  $\partial^a \tilde{\gamma}_{ab} = 0$ , where  $\tilde{\gamma}_{ab}$  is defined as

$$\tilde{\gamma}_{ab} := \gamma_{ab} - \frac{1}{2} \eta_{ab} \left( \gamma + 2 \tilde{\phi} \frac{F'_0}{F_0} \right), \quad (5.5)$$

the field equations (2.2) and (2.8) (for  $V \equiv 0$ ) become [49]

$$\square_\eta \tilde{\gamma}_{ab} = -16\pi \frac{G_0}{F_0} \tilde{T}_{ab}^{\text{matt}}, \quad (5.6)$$

$$\square_\eta \tilde{\phi} = 4\pi \zeta \frac{F'_0}{F_0} \tilde{T}^{\text{matt}}, \quad (5.7)$$

where  $\square_\eta$  is the D'Alembertian operator in the flat background metric, and the constant  $\zeta$  is defined as [49]

$$\zeta := \frac{1}{8\pi} \left( 1 + \frac{3(F'_0)^2}{16\pi F_0 G_0} \right)^{-1}. \quad (5.8)$$

Notice that the flat metric is used to raise and lower indices of first order tensorial quantities.

We will now perform the analysis of scalar gravitational waves in a spherical and vacuum spacetime, which is enough for the purpose of the following discussion. In that case one can neglect the tensor modes and assume that  $\tilde{\gamma}_{ab} \equiv 0$  (note that in spherical symmetry, quadrupole radiation is absent). Hence, according to equation (5.5) we obtain

$$\gamma_{ab} = -\tilde{\phi} \eta_{ab} \frac{F'_0}{F_0}. \quad (5.9)$$

Therefore, the whole metric at linear order reads

$$g_{ab} \approx (1 + \Phi) \eta_{ab}, \quad (5.10)$$

where  $\Phi := -\tilde{\phi} F'_0/F_0$  and the factor  $\epsilon$  has been re-absorbed in  $\tilde{\phi}$  (note that  $\tilde{\phi} \ll \phi_0$  (*i.e.*  $\Phi \ll 1$ )). The physical metric then turns out to be conformally flat,  $g_{ab} \approx \Omega^2 \eta_{ab}$ , with the conformal factor  $\Omega^2 := 1 + \Phi$ .

Gravitational waves are directly related with the Riemann tensor. Here we compute that tensor using the well-known relationship between two Riemann tensors associated with two conformal metrics (see *e.g.* Eq. (D.7) of Wald's [50]). In this case, the Riemann tensor associated with  $\eta_{ab}$  vanishes and, at linear order, we have

$$R_{Labc}{}^d = \delta^d_{[a} \nabla_{b]} \nabla_c \Phi - \eta^{de} \eta_{c[a} \nabla_{b]} \nabla_e \Phi, \quad (5.11)$$

where the subindex  $L$  indicates that this is valid only at the linear approximation. According to (5.11), we obtain the following components, which are directly related with the relative (tidal) acceleration between two particles in geodesic motion,

$$R_{L\,titj} = \frac{1}{2} \left( -\delta_{ij} \partial_{tt}^2 \Phi + \nabla_i \nabla_j \Phi \right). \quad (5.12)$$

Assuming now that  $\tilde{\phi} = \tilde{\phi}(t, r)$  is a spherically symmetric perturbation for the scalar field, we obtain

$$R_{L\,titj} = \frac{1}{2} \left[ -\delta_{ij} \partial_{tt}^2 \Phi + s_i s_j \partial_{rr}^2 \Phi + \frac{1}{r} (\delta_{ij} - s_i s_j) \partial_r \Phi \right]. \quad (5.13)$$

where  $s_i = \delta_{ij} x^j / r$  is a unit vector in the radial direction of propagation.

On the other hand, in vacuum and in spherical symmetry, the wave equation (5.7) implies

$$\partial_{tt}^2 \tilde{\phi} = \partial_{rr}^2 \tilde{\phi} + \frac{2}{r} \partial_r \tilde{\phi}. \quad (5.14)$$

Plugging (5.14) into (5.13) yields

$$\begin{aligned} R_{L\,titj} &= -\frac{1}{2} (\delta_{ij} - s_i s_j) \partial_{tt}^2 \Phi \\ &+ \frac{1}{2} (\delta_{ij} - 3s_i s_j) \frac{1}{r} \partial_r \Phi. \end{aligned} \quad (5.15)$$

For outgoing radiation  $\Phi(t, r) = \Psi(t - r)/r$ , thus the second term in (5.15), which involves the spatial derivative, will be very small with respect to the first one in the “wave zone” and so we can neglect it. Finally, we obtain the following expression

$$R_{L\,titj} \approx -\frac{1}{2} \perp_{ij} \partial_{tt}^2 \Phi, \quad (5.16)$$

where we have introduced the transverse projector  $\perp_{ij} = \delta_{ij} - s_i s_j$  in the orthogonal directions to  $s_i$  and neglected terms  $\mathcal{O}(1/r^2)$ . In the above expression, we have considered only the massless case. When the mass term is included, a *longitudinal* contribution appears in Eq. (5.16) (*c.f.* Ref. [21]).

According to (5.9), in the minimal coupling case, where  $F'_0 \equiv 0$ , or when one takes the value  $\phi_0 = 0$  asymptotically (like in the quadratic coupling  $F = 1 + 8\pi G_0 \xi \phi^2$ ), the scalar-gravitational waves are absent. However, taking for  $\phi_0$  the maximal value allowed by the Solar System experiments, which constrain  $\omega_{\text{BD}} > 4 \times 10^4$ , scalar gravitational waves are expected to develop in dynamical situations where the NMC scalar-field is non-zero initially, like in the IS phenomenon. We expect the amplitude of the  $1/r$ -contribution of the gravitational radiation to be of the following order

$$|R_{L\,titj}| \approx \frac{Q_{\text{scal}} \omega^2}{2D} |\perp_{ij}| |F'_0/F_0|, \quad (5.17)$$

where  $\omega$  is the frequency of the scalar wave,  $Q_{\text{scal}}$  is the scalar charge (which has units of mass) and  $D$  the distance to the source.

## VI. NUMERICAL SETUP

In this section we present the numerical ingredients that have been used in order to study the scalarization transition and the emission of scalar radiation in the boson star context.

### A. Formulation

We perform a numerical evolution of the equations of Sec. II B. However, since the ADM equations in GR are only weakly hyperbolic [51], we will use a formulation of the BSSN type, which has been particularly robust in the numerical evolution of both vacuum and matter spacetimes in GR [25, 26]. We adopt the particular version of the BSSN formulation presented in [52] that is specially adapted to spherical symmetry. In Appendix A we discuss the characteristic decomposition of this formulation for the case of an STT.

### B. Initial Data

We consider a single boson star in stationary equilibrium. In such a configuration the spacetime metric is time independent, and the scalar field  $\psi(t, r)$  oscillates in time with a fixed frequency  $\omega$ :

$$\psi(t, r) = \Psi(r) e^{i\omega t}. \quad (6.1)$$

In order to find the initial data one must substitute (6.1) into the KG Eq. (4.4). We now need to solve Eqs. (2.2) and (4.4) in order to obtain the frequency  $\omega$ , the function  $\Psi(r)$ , and the metric coefficients such that, for a given amplitude of the scalar field at the origin,  $\Psi(0)$ , the resulting spacetime is static. Following [36, 53, 54], we solve this problem in the polar-areal gauge, where the line element takes the form

$$ds^2 = -\alpha^2(r) dt^2 + A(r) dr^2 + r^2 d\Omega^2, \quad (6.2)$$

where  $d\Omega^2 = d\theta^2 + \sin^2(\theta) d\phi^2$  is the usual solid angle element. The field equations then reduce to:

$$\begin{aligned} \partial_r A &= A \left[ \frac{1-A}{r} + 4\pi r \left\{ 2AV_\psi + \frac{A\omega^2 \Psi^2}{\alpha^2} + Q_\psi^2 \right\} \right], \end{aligned} \quad (6.3)$$

$$\partial_r \alpha = \alpha \left[ \frac{A-1}{r} + \frac{\partial_r A}{2A} - 8\pi r AV_\psi \right], \quad (6.4)$$

$$\partial_r \Psi = Q_\psi, \quad (6.5)$$

$$\begin{aligned} \partial_r Q_\psi &= -Q_\psi \left[ \frac{2}{r} + \frac{\partial_r \alpha}{\alpha} - \frac{\partial_r A}{A} \right] \\ &+ A\Psi \left[ \partial_\psi V_\psi - \frac{\omega^2}{\alpha^2} \right], \end{aligned} \quad (6.6)$$



where the potential  $V_\psi$  is given by the Eq. (4.6). There are several solutions of the above system, depending on the value of the different variables at the origin and their asymptotic behavior. In order guarantee regularity at the origin we impose the following boundary conditions

$$A(0) = 1, \quad (6.7)$$

$$\partial_r \alpha|_{r=0} = 0, \quad (6.8)$$

$$\Psi(0) = \Psi_c, \quad (6.9)$$

$$Q_\psi(0) = 0, \quad (6.10)$$

Also, for the spacetime to be asymptotically flat we must ask for

$$A|_{\lim_{r \rightarrow \infty}} = 1, \quad (6.11)$$

$$\alpha|_{\lim_{r \rightarrow \infty}} = 1, \quad (6.12)$$

$$\Psi|_{\lim_{r \rightarrow \infty}} = 0. \quad (6.13)$$

One can consider this problem as an eigenvalue problem for  $\Psi(r)$  in the sense that, for a given value of the scalar field at the origin  $\Psi_c$ , the above system only admits solutions for a discrete set of frequencies  $\omega$ . We are interested in the ground state of the boson stars, which corresponds to the configuration with no nodes in  $\Psi(r)$ .

Numerical solutions of Eqs. (6.3-6.6) satisfying the boundary conditions (6.7-6.13), are obtained for a given value of  $\Psi_c$  by integrating the equations from the origin outwards using a shooting method [31]. This is similar to the case of neutron stars, where the integration is also performed outwards from the origin by giving a value of the energy-density at the center of the star. Fixing the value of the energy density at the center of the star is equivalent to choosing a particular stationary configuration, which in turn determines the ADM mass as well as the total number of particles (total baryon number in the case of neutron stars and total boson number in the case of boson stars).

Moreover, just like in neutron stars, one can construct a whole family of stationary configurations for different energy-densities at the origin. It can be shown that there is a specific value of the central density which maximizes the ADM mass. That point indicates the threshold to configurations that are unstable to gravitational collapse under small perturbations. Figure 1 shows the mass profile for a single boson star without self-interaction. The maximum mass configuration, which corresponds to a central value of the boson field given by  $\sigma(0) \sim 0.272$  [where  $\sigma(r) := \sqrt{4\pi G_0} \Psi(r)$  is a dimensionless boson field; *c.f.* Eq. (7.2) below], separates the space of configurations into two branches: the stable “S-branch”, and the unstable “U-branch”. When perturbed, configurations on the U-branch can either collapse to form black holes or disperse away depending on value of the binding energy [55].

In the case of STT, there is another point of instability towards spontaneous scalarization for a mass which is not the maximum one. In neutron stars there is a critical baryon mass below the maximum that marks the onset

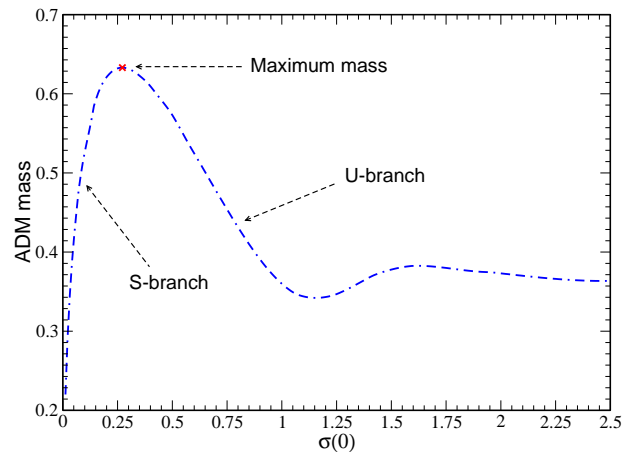


FIG. 1: ADM mass profile for a single boson star without self-interaction in GR, as a function of the central value of the boson field  $\sigma(0)$ . The maximum mass configuration, which corresponds to  $\sigma(0) \sim 0.272$ , separates the stable configurations (S-branch) from the unstable ones (U-branch).

of this instability. We expect that it is the total boson number that indicates the point of instability towards spontaneous scalarization. However, a priori this value is difficult to know unless one constructs a whole family of stationary configurations and looks for solutions with a non-trivial value of the non-minimal scalar field  $\phi$ . At this point is perhaps important to remark that a maximum mass model within STT usually corresponds to a model with a non-trivial scalar field. That is, it corresponds to a star that has already undergone a spontaneous scalarization process in which some of the scalar field has been radiated away and the star has reached a stationary configuration. This maximum mass star is then unstable and collapses to a black hole under a small perturbation (see Section VII).

## VII. NUMERICAL RESULTS

We performed numerical simulations of several single boson star configurations. We used the code described in [52], which consists of a spherical reduction of the BSSN formulation, coupled to the STT given by the Lagrangian (2.1). We have taken the non-minimal coupling function (2.7) to be of the form

$$F(\phi) = 8\pi f(\phi) = 1 + 8\pi G_0 \xi \phi^2, \quad (7.1)$$

with  $\xi$  a positive constant. In order to have a notation consistent with previous studies about boson stars [42, 55, 56], we define the dimensionless boson field

$$\sigma = \sqrt{4\pi G_0} \Psi. \quad (7.2)$$

All runs have been performed using a method of lines with a fourth order Runge-Kutta integration in time,

and fourth order centered differences in space. Constraint preserving boundary have been implemented using the algorithm described in Appendix B. Our typical simulations use a grid spacing of  $\Delta r = 0.048$ , and we take  $\Delta t = \Delta r/2$  in order to be sure that we satisfy the Courant-Friedrichs-Levy stability condition [51]. We have also performed some simulations with grid spacings of  $\Delta r = 0.024$  and  $\Delta r = 0.012$ , in which case the violations on the Hamiltonian constraint are dominated by spurious reflections from the boundary which are, in the worst case, of order  $10^{-9}$ . In all the runs presented here the outer boundaries are located at  $r_{out} = 240$ .

### A. Spontaneous Scalarization

The phenomenon of scalarization in compact objects and the emission of the monopolar gravitational waves depends strongly on the asymptotic value of the non-minimally coupled scalar field  $\phi$ . If the asymptotic value of  $\phi$  is zero, which corresponds to spontaneous scalarization, then  $F'$  tends to zero asymptotically which means that, according to (5.17), there are no monopolar gravitational waves. Nevertheless, it has been shown that in this case the evolution of stable boson stars on STT reaches a final state where the scalarization ensues [20]. Boson star configurations below a critical central value of the boson field  $\Psi_c^{\text{crit}}$  are stable with respect to Gaussian perturbations on the scalar field and do not lead to a SS transition: The scalar field  $\phi$  is just radiated away during the evolution. On the other hand, configurations above that critical value are unstable with respect to perturbations and undergo a transition to a scalarized state with a non-trivial scalar field  $\phi$  and a non-zero scalar charge.

### B. Induced scalarization

In the IS phenomenon, an initially non-zero and uniform NMC scalar field evolves naturally without the need of any perturbation. The reason for this is that for a non-zero background scalar field  $\phi(r) = \phi_0$  one finds  $F'(\phi)|_{\phi=\phi_0} \neq 0$ . The presence of the term  $f'R$  in the Klein-Gordon equation (2.3) then implies that this initial data will not be a stationary solution, and the field will therefore evolve away from its initial configuration without the need for an external perturbation. This is in contrast with the SS case for which we have initially  $\phi(r) = \phi_0 = 0$ , which is indeed a solution of Eq. (2.3), so an explicit perturbation is required to trigger the SS phenomenon.

Since in principle any background scalar field  $\phi_0$  in STT might disturb the constraints imposed by the Solar System experiments, the value of  $\phi_0$  must be chosen such that the corresponding Brans-Dicke parameter  $\omega_{\text{BD}}$  satisfies the observational bounds. Using the fact that the

parameter  $\omega_{\text{BD}}$  can be written as

$$\omega_{\text{BD}} = \left. \frac{f}{f'^2} \right|_{\phi_0} = \frac{1 + 8\pi G_0 \xi \phi_0^2}{32\pi G_0 \xi^2 \phi_0^2}, \quad (7.3)$$

where  $\xi$  is the NMC constant associated with the class of STT considered here, it turns out that

$$\phi_0 = \left| \frac{1}{\sqrt{8\pi\xi(4\omega_{\text{BD}}\xi - 1)}} \right|. \quad (7.4)$$

For a given value of  $\xi$ , one can then enforce the constraint  $\omega_{\text{BD}} \gtrsim 4.3 \times 10^4$  imposed by the Cassini probe [57], and use the above expression to fix the value for  $\phi_0$  that satisfies the observational bounds. In all the simulations discussed below we have chosen  $\phi_0$  in such a way as to saturate the Cassini bounds, that is, the one corresponding to  $\omega_{\text{BD}} = 4.3 \times 10^4$  (notice that  $\phi_0$  will then depend on the parameter  $\xi$ ).

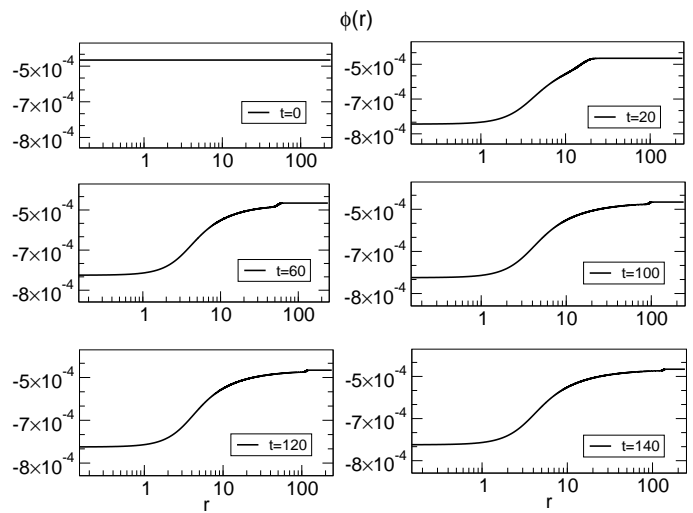


FIG. 2: Snapshots of the evolution of the NMC scalar field for the case when  $\sigma(0) \sim 0.266$  initially. For this simulation we have taken  $\xi = 1$ , and the NMC scalar field is initially set to  $\phi(r) = \phi_0 = -4.8 \times 10^{-4}$ , which corresponds to the background value that saturates the lower bound for  $\omega_{\text{BD}}$ . The system evolves until it reaches a quasi-stationary configuration with a non trivial scalar field  $\phi$ . This final configuration is what we refer to as “induced scalarization”. Notice that asymptotically  $\phi$  preserves its initial value  $\phi_0$ .

Figure 2 shows snapshots of the evolution of the NMC field  $\phi$  for a boson star with an initial central density  $\sigma(0) \sim 0.266$ , which is at the threshold of the unstable configurations. For this simulation the NMC parameter was taken to be  $\xi = 1$ , and the NMC scalar field is initially set to  $\phi(r) = \phi_0 = -4.8 \times 10^{-4}$ , which corresponds to the background value that saturates the lower bound for  $\omega_{\text{BD}}$ . In this case a quasi-stationary configuration with a non-trivial scalar field  $\phi$  is reached at the end of the simulation.

Figure 3 displays the initial and final states of the radial metric component  $A$ , the lapse function  $\alpha$ , the NMC

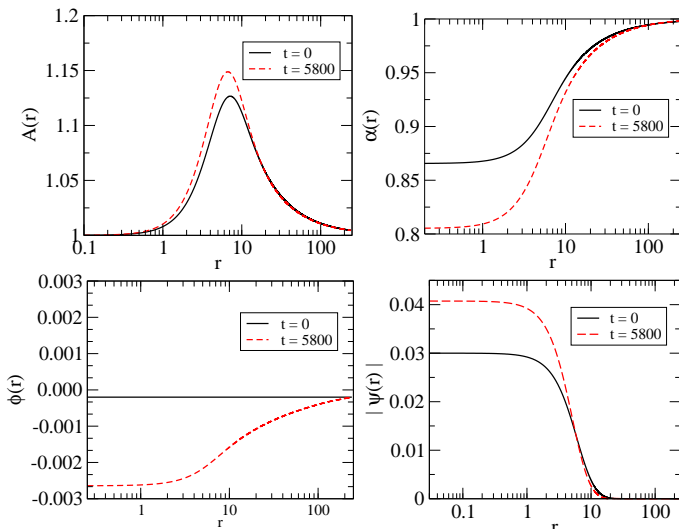


FIG. 3: Initial and final states of the radial metric component  $A$  (top left), lapse function  $\alpha$  (top right), the NMC field  $\phi$  (bottom left), and the norm of the complex bosonic field  $\Psi$  (bottom right), for an initial central density  $\sigma(0) \sim 0.106$  and  $\xi = 500$ . Just as in Fig. 2, the system undergoes scalarization and reaches a quasi-stationary configuration with a non-trivial NMC scalar field at the end of the evolution.

scalar field  $\phi$ , and the norm of the boson field  $|\Psi|$ , for a different simulation with  $\xi = 500$  and  $\sigma(0) = 0.106$  initially and  $\phi_0 = -9.6 \times 10^{-7}$ . Notice that, although the parameter  $\xi$  is much larger than in the previous case, the IS only seems to affect slightly the geometry of the space-time (confront, for example, the initial and final values of the lapse  $\alpha(0)$  in Fig. 3). In order to make this statement more precise, we first define an approximate size of our boson star  $R_{\text{star}}$  as the radius of the sphere which contains the 95% of the integrated mass. The *compactness* of the star is then defined as  $M_{\text{MS}}/R_{\text{star}}$ , with  $M_{\text{MS}}$  the Misner-Sharp mass of the system (see below). For the simulation of Figure 3 we find that the compactness of the star is reduced by only  $\sim 3\%$  with respect to its initial value.

The Misner-Sharp mass  $M_{\text{MS}}$  used to measure the mass of the system is defined as follows: Let  $r_a$  be the areal radial coordinate, we first define the “Misner-Sharp mass function”  $m_{\text{MS}}(r_a)$  in terms of the radial metric component  $g_{r_a r_a}(r_a)$  as [58]

$$m_{\text{MS}}(r_a) := \frac{r_a}{2} \left( 1 - \frac{1}{g_{r_a r_a}(r_a)} \right), \quad (7.5)$$

with  $r_a$  the areal radius. One can show that, for asymptotically-flat spherically-symmetric spacetimes, the Misner-Sharp mass function coincides with the ADM mass as long as we are in vacuum. That is, once we are in a region outside of all the sources we should find that  $m_{\text{MS}}(r_a)$  reaches a constant value  $M_{\text{MS}}$  such that  $M_{\text{MS}} = M_{\text{ADM}}$ .

Several considerations are now in order. First, even though our initial data is in the areal gauge, during the

evolution this is no longer the case, so that one must transform back from the radial coordinate  $r$  used in the simulation to the areal radius  $r_a$  in order to calculate the mass function. This is simple to do and we will not go into the details here. More important, however, is the fact that for boson stars we are never actually in vacuum since the bosonic field  $\Psi$  extends all the way to infinity. However, one finds that  $\Psi$  decays exponentially, so that in practice for stars that are not scalarized we very rapidly reach a region that for all practical purposes is indeed vacuum. For scalarized stars, on the other hand, we have to be more careful since the NMC field  $\phi$  decays more slowly (typically as  $\sim 1/r$ ), and in the IS case it in fact reaches a small non-zero asymptotic value  $\phi_0$ . This means that the Misner-Sharp mass function never quite reaches the constant “vacuum” value. Because of this, the values of  $M_{\text{MS}}$  we report actually correspond to the value of the mass function  $m_{\text{MS}}(r)$  evaluated at the boundary of the numerical grid. Strictly speaking this is not the actual mass of the system, but it is a good enough approximation for our purposes.

As a final comment one should also mention the fact that the Misner-Sharp mass  $M_{\text{MS}}$  only coincides with the ADM mass for static spacetimes. The spacetimes considered here are dynamic, and radiate energy during the scalarization process. When we talk about the initial and final mass we mean in fact the mass of the star, and not the “true” ADM mass which takes into account contributions all the way to infinity (and is therefore constant).

We will now try to understand the emergence of the scalarization phenomenon on energetic grounds, where stationary scalarized configurations turn out to be energetically preferred over unscalarized ones. For instance, it has been shown in the context of neutron stars [1, 18] that, beyond some critical baryon-mass, a stationary configuration with  $\phi \neq 0$  which maximizes the fractional binding-energy of the system, is energetically more favorable than the corresponding configuration at the same baryon mass with  $\phi \equiv 0$  (the GR case). This critical point depends on the details of the model, such as the value of  $\xi$ , the equation of state, etc.

Figure 4 shows the results of this energetic analysis for our scalarized boson stars. In the Figure we plot the fractional binding-energy  $(M_{\text{bos}}/M_{\text{MS}}) - 1$  as a function of the bosonic mass  $M_{\text{bos}}$  for several values of  $\xi$ . Here  $M_{\text{MS}}$  is calculated as described above, while  $M_{\text{bos}}$  is the mass contribution from the bosonic field alone obtained from Eq. (4.9). From the Figure one can see that, for a given value of  $M_{\text{bos}}$  and  $\xi$ , the scalarized configuration is energetically preferred when compared with an ordinary boson star with  $\phi \equiv 0$  (the GR case). It is important to mention here that, strictly speaking, this energetic analysis would only be valid for the SS case, where both the scalarized and unscalarized configurations have a vanishing asymptotic value of the NMC field  $\phi$ . Nevertheless, for small asymptotic values  $\phi_0$  one finds that bulk quantities are essentially the same in the IS and SS cases, so

one can still use the energetic argument.

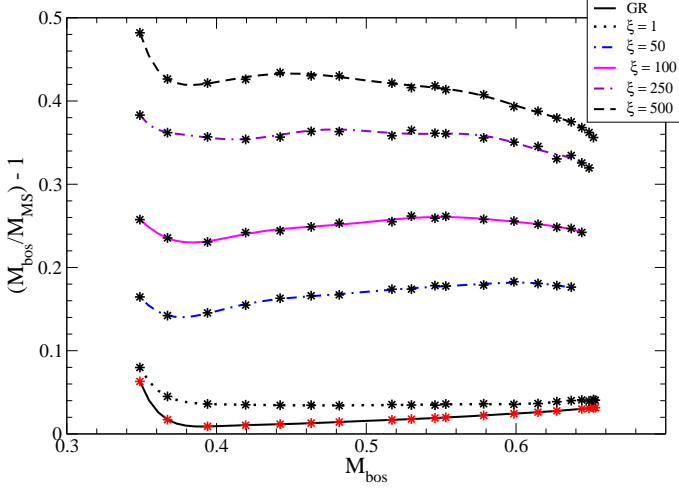


FIG. 4: Fractional binding energy  $(M_{\text{bos}}/M_{\text{MS}}) - 1$  as a function of the total boson mass  $M_{\text{bos}}$ , for both stationary scalarized and unscalarized (GR case) configurations. Configurations with larger binding energy are energetically preferred. The points correspond to the actual quasi-stationary final configurations resulting from our simulations, while the lines are a simple fit obtained with polynomial regression.

To corroborate the above analysis, in Figure 5 we plot the final value of the integrated scalar charge  $Q_{\text{scal}}$ , and the central absolute value of the NMC scalar field  $\phi$  (which always corresponds to its maximum), for several sets of boson star configurations with different values of the parameter  $\xi$  as a function of the initial central density of the star  $\sigma(0)$ . We have chosen initial configurations with central density in the interval  $[0.028, 0.265]$ , which correspond to boson stars which in GR are stable against gravitational collapse (*i.e.* the S-branch configurations of Fig. 1). For these configurations we have always assumed  $\omega_{\text{BD}} = 4.0 \times 10^4$ , which fixes the asymptotic value of the NMC field  $\phi_0$ . As expected, these stars evolve to a quasi-stationary final state with a non-trivial scalar field  $\phi$ . We can conclude that the scalarization phenomenon depends strongly on the value of the parameter  $\xi$ . For all configurations that we have analyzed we find that the final value of the scalar charge, as well as the central value of  $\phi$ , reach a maximum for  $\xi \sim 50$ . Notice also that the final central value of the NMC scalar field seems to depend logarithmically on the central density of the initial boson star  $\sigma(0)$  (in Fig. 5 we use a log scale for  $\sigma(0)$  in order to see this logarithmic dependence).

### C. Gravitational collapse and black hole formation

Since the scalarization phenomenon modifies the compactness of the star, one would expect that the threshold to the U-branch associated with the scalarized stars also changes depending on the value of  $\xi$ . For instance, the initial unscalarized configuration with  $\sigma(0) \sim 0.266$  and

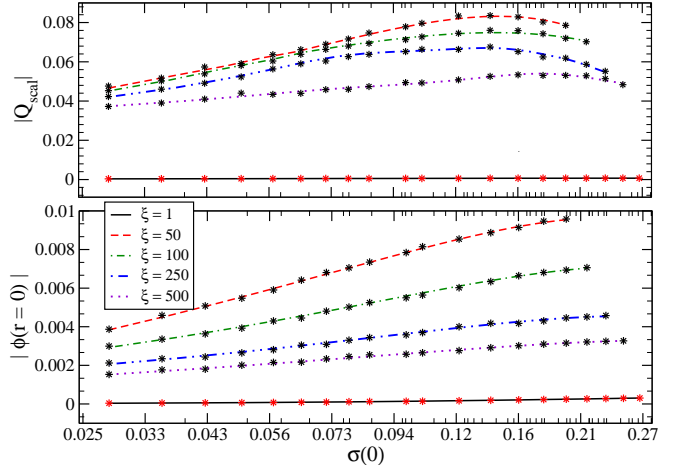


FIG. 5: Scalar charge (top panel), and central absolute value of the NMC scalar field (bottom panel), for stable boson star configurations as a function of the initial central density of the boson field  $\sigma(0)$  and different values of  $\xi$ . Notice the logarithmic scale in  $\sigma(0)$ .

$\xi = 1$ , which evolved into a quasi-stationary scalarized state as depicted in Fig. 2, will collapse into a black hole if we take instead  $\xi \geq 10$ . This means that the critical  $\sigma_{\text{crit}}(0)$  seems to decrease when compared to the GR case in a way that depends on the value of the parameter  $\xi$ . In particular, we have found that for  $\xi = 50$ , the last scalarized boson star configuration that is stable against black hole formation corresponds to a central value  $\sigma(0) \sim 0.195$ . This value of  $\sigma(0)$  has to be contrasted with the value  $\sigma(0) \sim 0.272$  for  $\xi = 0$  (the GR case), which is associated with the usual maximum mass configuration. In summary, depending on the value of  $\xi$ , there are two kinds of instabilities for boson stars in STT: On the one hand, there is an instability that takes the star into a stable scalarized state and, on the other hand, an instability that causes a scalarized star to collapse to a black hole. Presumably, an unscalarized boson star that collapses directly into a black hole may also reach a transient (possibly very brief) state of scalarization before collapsing.

We have studied the dynamical collapse of boson stars in STT toward a black hole. In order to be sure that a black hole is formed, we look for the appearance of an apparent horizon during the simulations. As expected, for unstable configurations an apparent horizon appears suddenly after some evolution. Its area then grows for some time as more matter is accreted, until it finally settles once all the initial matter has either fallen into the black hole or has been radiated away. Figure 6 shows the apparent horizon mass (defined in terms of its area  $A$  as  $M_{\text{AH}} = \sqrt{A/16\pi}$ ) as a function of time, for the first unstable boson star configuration for  $\xi = \{1, 50, 250, 500\}$  and  $\sigma(0) = \{0.268, 0.195, 0.231, 0.249\}$ . These values of the central density are above the threshold given by Table I. The asymptotic value of the NMC field  $\phi_0$  is dependent



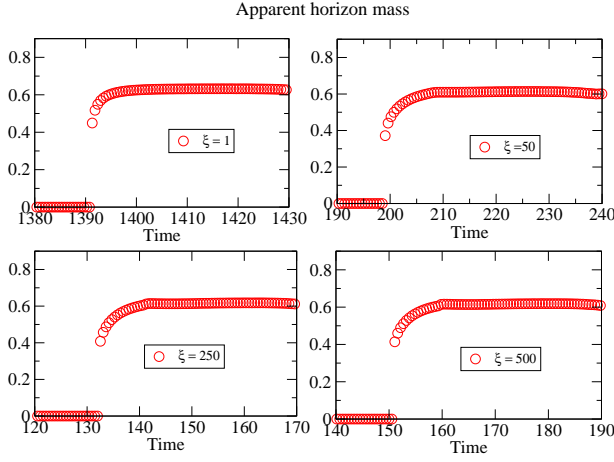


FIG. 6: Apparent horizon mass of the first scalarized unstable boson star configurations for different values of the parameter  $\xi$ . When  $\xi = 1$  the configuration is essentially that of GR. For  $\xi = \{50, 250, 500\}$  the scalarized boson star collapses toward a black hole of the same mass but at much earlier times.

of  $\xi$  through Eq. (7.4). Notice that as  $\xi$  increases, the black hole formation time first decreases up to a certain value of  $\xi$ , after which the time of collapse increases again for larger  $\xi$ .

Figure 7 shows some snapshots of the evolution of the NMC scalar field for a case where  $\sigma(0) = 0.23$  and  $\xi = 50$ , and an asymptotic value of  $\phi_0 = -9.25 \times 10^{-11}$ . A similar initial configuration with  $\xi = 0$  (the GR case) is stable, while configurations with  $\xi < 50$  evolve into a stable scalarized state.

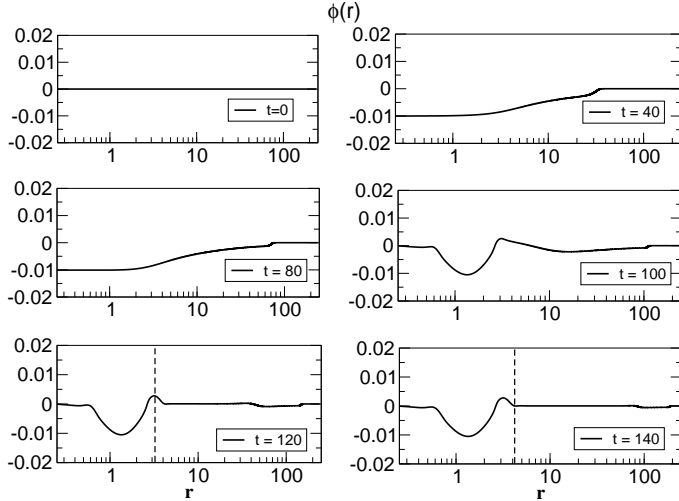


FIG. 7: Snapshots of the evolution of the NMC scalar field for an initial configuration with  $\sigma(0) = 0.230$  and  $\xi = 50$ . The star eventually collapses into a black hole. The same initial configuration with  $\sigma(0) = 0.230$ , but taking  $\xi = 0$  (the GR case), is stable. The vertical lines in the bottom panels indicate the location of the apparent horizon.

## D. Scalar radiation

Gravitational radiation can carry energy away from an isolated system, and it also encodes important information about the physical properties of the system itself. In [59], Harada *et al* have performed a numerical study of the scalar gravitational radiation emitted during an Oppenheimer-Snyder collapse in STTs in terms of the initial parameters, such as the initial radius and mass of the dust.

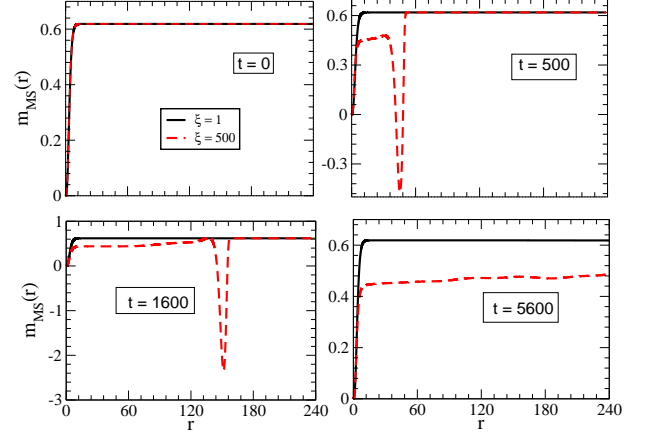


FIG. 8: Evolution of the Misner-Sharp mass for a stable boson star with central density  $\sigma(0) \sim 0.141$ . The variation of the Misner-Sharp mass with  $\xi = 1$  is insignificant while the variation of the mass with  $\xi = 500$  is around 20% (see table I). Notice however that the peak in the plots is not physical since  $m_{MS}$  acquires a physical meaning only in the limit  $r \rightarrow \infty$ .

In order to study the emission of scalar gravitational radiation in our boson star configurations, we will start by considering the reduction of the Misner-Sharp mass during the scalarization process. Figure 8 displays the evolution of the mass function  $m_{MS}(r)$  for an initial boson star configuration with central density  $\sigma(0) \sim 0.141$ , both for  $\xi = 1$  and  $\xi = 500$ . It is clear that the configuration with  $\xi = 1$  reaches rapidly a quasi-stationary state where the variation of the Misner-Sharp mass can be ignored (it is less than 1%). On the other hand, the evolution for the configuration with  $\xi = 500$  is quite different. First, one can notice a distortion moving outward for which the mass function even becomes negative. The position of this distortion can be seen to coincide with an outward moving pulse of scalar field  $\phi$ . One should not worry about the fact that the mass function is negative since, as we have said before, one can only interpret this as a mass in the vacuum regions. More importantly, once this pulse has moved away, we can see a very clear reduction in the mass function. At the end of the simulation, the final reduction in the mass is of around 20% (see table I). We should also mention the fact that in this case the metric components and the scalar field  $\phi$  continue to oscillate at late times around a fixed configuration (these oscillations are quite independent of the resolution of the

numerical evolution).

One could naively think that this reduction in the mass is entirely produced by the emission of scalar *gravitational* radiation. However, at this point it is difficult to separate between the total amount of energy carried away by the scalar field  $\phi$  and that carried by the scalar gravitational radiation itself. The latter of course arises due to the NMC between the scalar field and the curvature, but everything is mixed in the flux of energy as given by Eq. (2.20). For instance, in the SS case with  $\phi_0 = 0$  some

scalar field is still radiated away during the transition to the quasi-stationary scalarized state (or during the collapse to a black hole), even though in that case we do not expect scalar gravitational radiation since  $F'(\phi)_{\phi=0} \equiv 0$ . In order to have an unambiguous quantification of the amount of energy emitted in the form of scalar gravitational radiation one would need to go to second order perturbation theory and compute the equivalent of the Isaacson energy-momentum tensor in STT. We will leave this computation for a future work.

$\sigma(0)$	$\xi / \phi_0$	$M_{in}$	$M_{fin}$	$(M_{fin} - M_{in})$	$E_{flux}$
0.267	$1 / -4.8 \times 10^{-4}$	$6.329 \times 10^{-1}$	$6.325 \times 10^{-1} \pm 1.81 \times 10^{-4}$	$4.000 \times 10^{-4}$	$9.290 \times 10^{-6} \pm 1.41 \times 10^{-8}$
0.194	$50 / -9.6 \times 10^{-6}$	$6.189 \times 10^{-1}$	$5.826 \times 10^{-1} \pm 3.55 \times 10^{-3}$	$3.630 \times 10^{-2}$	$3.725 \times 10^{-2} \pm 3.41 \times 10^{-3}$
0.212	$100 / -4.8 \times 10^{-6}$	$6.251 \times 10^{-1}$	$5.611 \times 10^{-1} \pm 3.00 \times 10^{-3}$	$6.400 \times 10^{-2}$	$6.183 \times 10^{-2} \pm 3.37 \times 10^{-3}$
0.230	$250 / -1.9 \times 10^{-6}$	$6.293 \times 10^{-1}$	$5.260 \times 10^{-1} \pm 3.80 \times 10^{-3}$	$1.033 \times 10^{-1}$	$1.020 \times 10^{-1} \pm 3.42 \times 10^{-3}$
0.248	$500 / -9.6 \times 10^{-7}$	$6.320 \times 10^{-1}$	$5.050 \times 10^{-1} \pm 2.84 \times 10^{-3}$	$1.270 \times 10^{-1}$	$1.271 \times 10^{-1} \pm 1.45 \times 10^{-3}$

TABLE I: Initial and final values of the Misner-Sharp mass and integrated energy flux of the last stable boson star configuration in SST as measured by an Euler observer, for different values of  $\xi$  which, according to Eq. (7.4), correspond to different values of  $\phi_0$ .

Figure 9 shows the final Misner-Sharp mass for a sequence of boson star configurations both in GR ( $\xi = 0$ ), and for STT with different values of  $\xi$ . The configurations presented here correspond to the S-branch of a single boson star for which the system has reached a stationary state. The stationary unstable configurations (*i.e.* the U-branch) would continue on the right after the last plotted point of the curves. We have performed several numerical simulations using central amplitudes beyond the new S-branch in STT, and we have confirmed that the stars collapse into a black hole.

Table I summarizes the initial and final states of the last stable boson star configurations found for each curve of Fig. 9. Notice that for many of the cases studied here, at late times the system reaches a oscillating state, with oscillations that seem to decay very slowly, which makes it difficult to determine the final value of the Misner-Sharp mass. So, in order to provide an error estimation on the values reported on it, we consider a time average between the maximum and minimum value of the “final” mass. We also include the value of the integrated energy flux as measured by an Eulerian observer. Notice that the difference between the initial and final masses agrees very well with the energy flux for almost all the values of  $\xi$ , except for  $\xi = 1$ . In this case the oscillations of the system do not allow us to get an accurate value for the final mass of the system.

The evolution of the stars considered above proceeds in general as follows: After the initial burst of scalar radi-

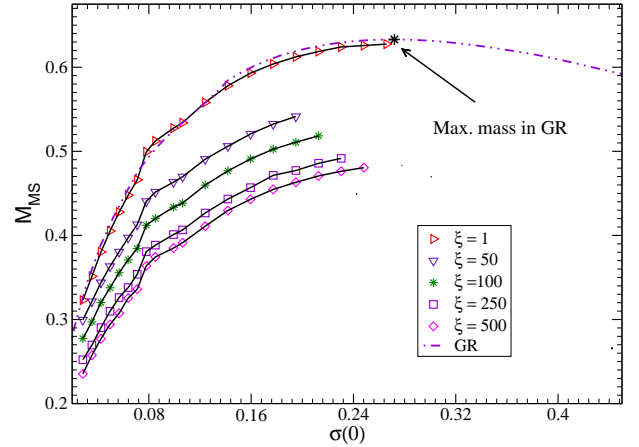


FIG. 9: Misner-Sharp mass for a sequence of stable stationary scalarized boson stars for different values of  $\xi$ . For reference we also show the GR configurations ( $\xi = 0$ ). The last point on every curve corresponds to the last stable configuration found. To the right of that point all configurations are unstable.

ation due to the scalarization process, the system settles down and reaches a state with very long-lived oscillations with a characteristic frequency. In the bottom panel of Figure 10 we show the main frequencies of this oscillations for the stable configurations presented in Fig. 9. We obtain these frequencies by performing a discrete Fourier transform in time (at late times) of the non-minimal

scalar field at a fixed radius  $r = 120$ , and looking for the largest peak. One would expect that the scalar gravitational waves should have the same frequency [59]. Notice that the main frequency of the system seems to be independent of the parameter  $\xi$ . The top panel of the Figure shows the actual Fourier transform (the power spectrum) for the case  $\phi_0 = 0.07$  where one can see that there is indeed a very clear peak.

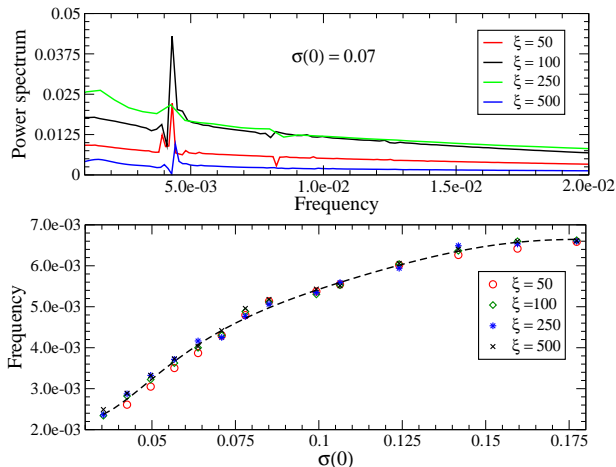


FIG. 10: *Top panel:* Fourier transform in time of the NMC scalar field evaluated at  $r = 120$  for different values of  $\xi$  at late times (after the scalarization process). The initial configuration corresponds to a boson star with  $\sigma(0) = 0.07$ . *Bottom panel:* Main frequencies (peaks in the power spectrum) for different values of  $\sigma(0)$ . Notice that these frequencies seem to be independent of the parameter  $\xi$ .

### VIII. CONCLUSIONS

Boson stars are stable self-gravitational configurations of a complex massive scalar field that evolves according to the Klein-Gordon equation. The expected mass of these type of stars typically varies between the mass of an asteroid and a few solar masses, depending on the mass parameter of the bosonic scalar field, some solar masses [38]. Though hypothetical, boson stars are simple models that can be used to understand the corrections to general relativity proposed by alternative theories of gravity. Any alternative theory of gravity has to be tested against observations, both at the scale of the solar system and at the cosmological scale. Scalar-tensor theories of gravity, where a (real) scalar field is non-minimally coupled to gravity, are interesting generalizations of general relativity that have so far not been ruled out by observations.

In this paper we have used a scalar tensor theory of gravity to study the evolution of distinct families of single boson stars parameterized by the central density of the star and the parameter  $\xi$  that controls the non-minimal coupling of the theory. We have focused on the transition to a scalarized state using a fully relativistic code in

spherical symmetry. We have found that, just as it happens with neutron stars, boson stars can also undergo both spontaneous and induced scalarization, the latter case linked directly with the emission of scalar (monopolar) gravitational waves.

Our numerical experiments show that the final magnitude of the non-minimally coupled scalar field seems to depend logarithmically on the central density of the boson star. We have also found that there is a critical value of the non-minimal coupling parameter  $\xi$ , corresponding to about  $\xi \sim 50$ , that maximizes the scalarization (*i.e.* the amount of final scalar charge). On the other hand, the maximum reduction of the initial mass of the boson star (about 20%), due to energy radiated to infinity during the scalarization process, was obtained for the maximum value of the parameter  $\xi$  considered in our evolutions ( $\xi = 500$ ). We summarized our results in Table I. Each configuration considered there corresponds to the critical density that separates the stable and unstable branches of a single boson star in scalar tensor theories for different values of  $\xi$ . Figure 9 shows the stable branches as a function of this parameter, once the system has reached final quasi-stationary state. It is evident that, whereas a small value of  $\xi$  leads to results that are very close to those of general relativity ( $\xi = 0$ ), larger values lead to important deviations that in principle could be measured.

At this point it is important to stress the fact that in all the evolutions presented here there are two parameters associated with the specific form of the scalar tensor theory: The free parameter  $\xi$  used in the expression for the non-minimal coupling function  $F(\phi) = 1 + 8\pi G_0 \xi \phi^2$ , and the asymptotic (cosmological) value of the scalar field  $\phi_0$  that in our evolutions is chosen as the maximum value allowed by the constraints imposed by the Cassini probe on the effective Brans-Dicke parameter [given by Eq. (7.3)]. This ensures that all our results satisfy the bounds imposed by the Solar System experiments.

Finally, we have taken a first step in trying to characterize the monopolar gravitational waves emitted during the scalarization process. One would expect that the magnitude of this monopolar radiation will be proportional to the product of the scalar charge and the square magnitude of the frequency of the radiation. We have found that this frequency seems to be independent of the coupling parameter  $\xi$ .

### Appendix A: Characteristic Variables for the BSSN Formulation in STT

Using the slicing condition (2.26), and assuming that the shift vector is an *a priori* given function of the coordinates, Salgado *et al.* have presented the characteristic decomposition of the BSSN formulation in the STT context [27]. They have shown that this formulation leads to a well-posed Cauchy problem in the Jordan frame. In this appendix we show that the algorithm used for deal-

ing with the regularization of the origin, in which one introduces a set of auxiliary variables to impose all the required regularity conditions [20, 60, 61], does not spoil those results.

Let us start by considering the spatial metric in spherical coordinates written in the form

$$dl^2 = A(t, r)dr^2 + r^2 B(t, r)d\Omega^2 \quad (\text{A1})$$

$$= e^{4\chi} [a(t, r)dr^2 + r^2 b(t, r)d\Omega^2], \quad (\text{A2})$$

where  $e^\chi$  is the conformal factor and  $d\Omega^2$  the standard solid angle element. In order to construct a fully first order and regularized BSSN system, one first needs to introduce the following set of variables

$$d_\alpha = \partial_r \ln \alpha, \quad d_a = \frac{1}{2} \partial_r \ln a, \quad (\text{A3})$$

$$d_\lambda = \partial_r \lambda, \quad \Upsilon = \partial_r \chi, \quad (\text{A4})$$

$$\hat{\Delta}^r = \frac{1}{a} \left( \frac{\partial_r a}{2a} - \frac{\partial_r b}{b} - 2r\lambda \right), \quad (\text{A5})$$

where  $\lambda$  is defined below in Eq. (A15). It turns out that, with the above variables, the *principal* part of the BSSN formulation in the STT context, coupled with the slicing condition (2.26), is given by

$$\partial_0 d_\alpha \simeq -\alpha f_{\text{BM}} \left( \partial_r K - \frac{\theta f'}{f_{\text{BM}} f} \partial_r \Pi \right), \quad (\text{A6})$$

$$\partial_0 \Upsilon \simeq -\frac{1}{6} \alpha \partial_r K, \quad (\text{A7})$$

$$\partial_0 d_a \simeq -\frac{2}{3} \alpha r^2 \partial_r A_\lambda, \quad (\text{A8})$$

$$\partial_0 K \simeq -\frac{\alpha e^{-4\chi}}{a} \left( \partial_r d_\alpha - \frac{f'}{f} \partial_r Q_r \right), \quad (\text{A9})$$

$$\begin{aligned} \partial_0 A_\lambda \simeq & -\frac{\alpha e^{-4\chi}}{r^2 a} \left( \partial_r d_\alpha + 2 \partial_r \Upsilon - \frac{b r^2}{2a} \partial_r d_\lambda \right. \\ & \left. - a \partial_r \hat{\Delta}^r + \frac{f'}{f} \partial_r Q_r \right), \end{aligned} \quad (\text{A10})$$

$$\partial_0 d_\lambda \simeq \frac{2\alpha a}{b} \partial_r A_\lambda, \quad (\text{A11})$$

$$\begin{aligned} \partial_0 \hat{\Delta}^r \simeq & \frac{2\alpha r^2}{3a} (\eta - 2) \partial_r A_\lambda - \frac{2\alpha \eta}{3a} \partial_r K \\ & + \frac{\alpha \eta f'}{a f} \partial_r \Pi, \end{aligned} \quad (\text{A12})$$

$$\partial_0 Q_r \simeq \alpha \partial_r \Pi, \quad (\text{A13})$$

$$\partial_0 \Pi \simeq \frac{\alpha e^{-4\chi}}{a} \partial_r Q_r, \quad (\text{A14})$$

where we have defined  $\partial_0 = \partial_t + \beta^r \partial_r$ .

Notice that Eqs. (A13-A14) are the spherical reduction of the Eqs. of motion (2.14-2.15). Moreover, the quantities  $\lambda$  and  $A_\lambda$  are auxiliary variables needed in order to impose regularity conditions at the origin, and which are defined by [20]

$$\lambda := \frac{1}{r^2} (1 - a/b), \quad A_\lambda = \frac{1}{r^2} (A_a - A_b). \quad (\text{A15})$$

Also, the equation of motion for  $\hat{\Delta}^r$  has been modified by adding a multiple of the momentum constraint which is controlled by the  $\eta$  parameter. In the following, we consider, for simplicity, that  $\eta = 2$  (see [20]).

Taking into account the fact that an evolution system of the form

$$\partial_t u = \nu_1 \partial_r v, \quad \partial_t v = \nu_2 \partial_r u, \quad (\text{A16})$$

has the characteristic variables  $w_\pm = u \mp \sqrt{(\nu_2/\nu_1)} v$  with characteristic speeds  $\pm \sqrt{\nu_1 \nu_2}$ , it is easy to show that the subsystem (A13-A14) has the characteristic decomposition

$$U_\pm^\phi = Q_r \pm e^{2\chi} \sqrt{a} \Pi, \quad (\text{A17})$$

with speeds of propagation

$$\mu_\pm^\phi = \beta^r \mp \alpha \frac{e^{-2\chi}}{\sqrt{a}}. \quad (\text{A18})$$

On the other hand, the characteristic variables related with the choice of slicing, and associated with the subsystem (A6) and (A9), turn out to be

$$\begin{aligned} U_\pm^{\text{gauge}} = & d_\alpha \pm \alpha e^{2\chi} \sqrt{a f_{\text{BM}}} K + \frac{f'}{f(1 - f_{\text{BM}})} \\ & \times \{Q_r(f_{\text{BM}} - \theta) - e^{2\chi} \sqrt{a f_{\text{BM}}(1 - \theta)} \Pi\}, \end{aligned} \quad (\text{A19})$$

with characteristic speeds

$$\mu_\pm^{\text{gauge}} = \beta^r \mp \alpha \frac{\sqrt{f_{\text{BM}}} e^{-2\chi}}{\sqrt{a}}. \quad (\text{A20})$$

Furthermore, the following combinations

$$\begin{aligned} U_\pm^\lambda = & d_\lambda \pm \frac{f' \{Q_r(1 - 2f_{\text{BM}} + \theta) - \sqrt{a} e^{2\chi}(1 - \theta) \Pi\}}{2f(1 - f_{\text{BM}})} \\ & - \frac{1}{2} \sqrt{a} e^{2\chi} (K - A_\lambda r^2) \mp \frac{a}{2} \left( \hat{\Delta}^r + \frac{r^2 d_\lambda}{2a^{5/2}} \right), \end{aligned} \quad (\text{A21})$$

provide two more characteristic variables with associated speeds

$$\mu_\pm = \beta^r \mp \alpha \frac{e^{-2\chi}}{\sqrt{a}}. \quad (\text{A22})$$

Finally, the following variables

$$U_1^0 = \hat{\Delta}^r - \frac{2f' Q_r}{a f} \left( 1 - \frac{2\theta}{3f_{\text{BM}}} \right) - \frac{4d_\alpha}{3a f_{\text{BM}}}, \quad (\text{A23})$$

$$U_2^0 = -a \hat{\Delta}^r + \frac{f' Q_r (2f' f_{\text{BM}} - \theta)}{f f_{\text{BM}}} + \frac{d_\alpha}{f_{\text{BM}}} + 2\Upsilon, \quad (\text{A24})$$

$$U_3^0 = -U_2 + \frac{1}{2} \left( 3d_a + \frac{r^2 d_\lambda}{a^{3/2}} \right), \quad (\text{A25})$$

are the remaining characteristic variables with speed  $\beta^r$ .



## Appendix B: Constraint preserving boundary conditions

To reduce the influence of the numerical boundary on the dynamics of the system we have considered constraint preserving boundary conditions (CPBC), in the sense that small violations of the constraints introduced by spurious reflections from the boundary converge away with the resolution. This is not only motivated by the requirement of having a well-posed initial boundary problem, but mainly because for long evolutions such as those considered here, constraint violating modes may propagate inside the domain contaminating the interior solution, which could lead to an incorrect physical interpretation [62].

In order to impose our CPBCs we introduce information from the characteristic variables at the boundary through the following algorithm.

1. We construct numerically the characteristic outgoing modes  $U_+$  using the dynamical variables, such as gauge, metric components and  $\phi$ , at the boundary. For instance, one can reconstruct the outgoing mode  $U_+^\phi$  at the boundary by using one-sided difference scheme for  $\Pi$  and  $Q_r$ .
2. In order to reconstruct the incoming scalar and gauge fields,  $U_-^\phi$  and  $U_-^{\text{gauge}}$ , we assume that  $\phi$  and  $\alpha$  behave at the boundary as outgoing spherical waves of the form:

$$u(t, r) = u_0 + \frac{1}{r} f(r - t), \quad (\text{B1})$$

with  $u_0$  their corresponding asymptotic values. By taking time and space derivatives one can then reconstruct the corresponding incoming characteristic fields. For example, for  $U_-^\phi$  we find (assuming that  $\phi = 0$  asymptotically):

$$U_-^\phi = -\frac{e^{-2\chi}}{\sqrt{ar}} \phi. \quad (\text{B2})$$

It is interesting to notice that the incoming fields are *not* zero, as one could naively expect (just setting them to zero introduces quite large reflections).

3. This leaves us with the incoming field  $U_-^\lambda$ . This is where one can impose the constraints, as one can show that the spatial derivative  $\partial_r U_-^\lambda$  can be written as a combination of the constraints plus a term that contains no derivatives of the dynamical variables. Asking then for the constraints to vanish at the boundary allows us to evaluate  $\partial_r U_-^\lambda$  directly at the boundary. And once we have  $\partial_r U_-^\lambda$  at the boundary we can use it, together with the values of  $U_-^\lambda$  at the nearby points, to solve for  $U_-^\lambda$  at the boundary by simple finite differencing.

4. Finally, we recover the dynamical variables using both the incoming and outgoing modes. Notice that it is not necessary to recover all the variables, since many of them are in fact not independent.

The above algorithm allows us to impose CPBCs for the spherical reduction of the BSSN formulation. As an example, in Figure 11 we show results from an evolution of a single boson star using forth order spatial differences and a forth order Runge-Kutta for the integration in time. The outer boundary is located at  $r_{\text{out}} = 240$ . The figure shows the  $L_2$  norm of the violation of the Hamiltonian and momentum constraints for a boson star with  $\sigma(0) = 0.1$ , and for two different resolutions. Notice that while the light crossing time of the numerical grid is  $t \sim 240$ , the scheme remains fourth order convergent for much longer times. The boundary conditions do a spurious reflection whose magnitude is less than  $10^{-9}$ . This effect is only evident in the momentum constraint at  $t = 240$  and  $t = 480$ . The magnitude of the violation of the Hamiltonian constraint in the interior is much larger than those reflections.

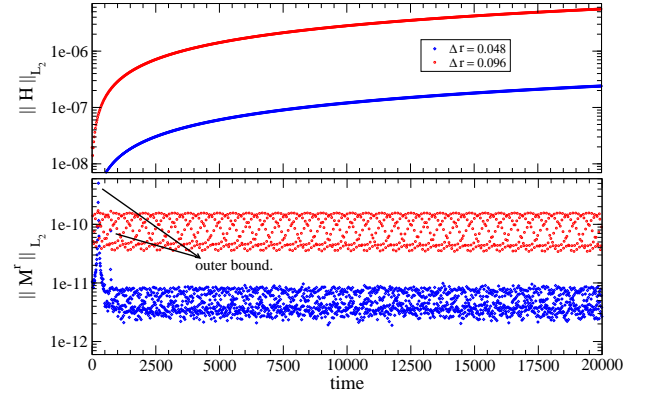


FIG. 11: Violation of the constraints for a boson star with  $\sigma(0) = 0.1$ . The  $L_2$  norm of the Hamiltonian (top panel) and the momentum constraints (bottom panel) is plotted for two different resolutions as a function of the time. The effect of the outer boundary conditions is visible only in the momentum constraint at times  $t = 240$  and  $t = 480$ .

## Acknowledgments

This work was supported in part by CONACyT grants SEP-2004-C01-47209-F, 82787, 149945 and 132132, and by DGAPA-UNAM through grant IN115310. JCD acknowledges DGAPA-UNAM for postdoctoral grant. MR was supported by Spanish Ministry of Science and Innovation under grants CSD2007-00042, CSD2009-00064 and FPA2010-16495, and Govern de les Illes Balears.

- 
- [1] T. Damour and G. Esposito-Farèse, *Class. Quantum Grav.* **9**, 2093 (1992).
- [2] Y. Fujii and K. Maeda, *The Scalar-Tensor Theory of Gravitation* (Cambridge University Press, Cambridge, England, 2003).
- [3] P. Jordan, Friedrich Vieweg und Sohn, Braunschweig (1955).
- [4] C. Brans and C. H. Dicke, *Phys. Rev.* **124**, 925 (1961).
- [5] C. M. Will, *Living Rev. Rel.* **9**, 3 (2005), an update of the Living Review article originally published in 2001, gr-qc/0510072.
- [6] T. Damour and G. Esposito-Farèse, *Phys. Rev.* **D54**, 1474 (1996).
- [7] F. Perrotta, C. Baccigalupi, and S. Matarrese, *Phys. Rev.* **D61**, 023507 (1999), astro-ph/9906066.
- [8] B. Boisseau, G. Esposito-Farèse, D. Polarski, and A. A. Starobinsky, *Phys. Rev. Lett.* **85**, 2236 (2000).
- [9] L. Amendola, *Phys. Rev. Lett.* **86**, 196 (2001).
- [10] A. Riazuelo and J. P. Uzan, *Phys. Rev.* **D66**, 023525 (2002).
- [11] M. Salgado (Frontier Group, Paris, France, 2002).
- [12] C. Schmid, J. P. Uzan, and A. Riazuelo, *Phys. Rev.* **D71**, 083512 (2005).
- [13] T. Damour and G. Esposito-Farèse, *Phys. Rev. Lett.* **70**, 2220 (1993).
- [14] T. Harada, *Prog. Theor. Phys.* **98**, 359 (1997).
- [15] T. Harada, *Phys. Rev.* **D57**, 4802 (1998).
- [16] J. Novak, *Phys. Rev.* **D58**, 064019 (1998), gr-qc/9806022.
- [17] T. Damour and G. Esposito-Farèse, *Phys. Rev.* **D58**, 042001 (1998).
- [18] M. Salgado, D. Sudarsky, and U. Nucamendi, *Phys. Rev.* **D58**, 124003 (1998), gr-qc/9806070.
- [19] A. W. Whinnett, *Phys. Rev.* **D61**, 124014 (2000), gr-qc/9911052.
- [20] M. Alcubierre, J. C. Degollado, D. Nunez, M. Ruiz, and M. Salgado, *Phys. Rev.* **D81**, 124018 (2010), 1003.4767.
- [21] M. Maggiore and A. Nicolis, *Phys. Rev.* **D62**, 024004 (2000).
- [22] J. Novak, *Phys. Rev.* **D57**, 4789 (1998), gr-qc/9707041.
- [23] H. Sotani and K. D. Kokkotas, *Phys. Rev.* **D71**, 124038 (2005), gr-qc/0506060.
- [24] M. Salgado, *Class. Quantum Grav.* **23**, 4719 (2006), gr-qc/0509001.
- [25] M. Shibata and T. Nakamura, *Phys. Rev.* **D52**, 5428 (1995).
- [26] T. W. Baumgarte and S. L. Shapiro, *Phys. Rev.* **D59**, 024007 (1998), gr-qc/9810065.
- [27] M. Salgado, D. M.-d. Rio, M. Alcubierre, and D. Nunez (2008), 0801.2372.
- [28] J. York, in *Sources of Gravitational Radiation*, edited by L. Smarr (Cambridge University Press, Cambridge, England, 1979).
- [29] E. Gourgoulhon, *3+1 Formalism in General Relativity, Bases of Numerical Relativity* (Springer, Heidelberg, Germany, 2012).
- [30] C. Bona, J. Massó, E. Seidel, and J. Stela, *Phys. Rev. Lett.* **75**, 600 (1995), gr-qc/9412071.
- [31] W. H. Press, B. P. Flannery, S. A. Teukolsky, and W. T. Vetterling, *Numerical Recipes* (Cambridge University Press, Cambridge, England, 1986).
- [32] P. Pani, V. Cardoso, E. Berti, J. Read, and M. Salgado, *Phys. Rev.* **D83**, 081501 (2011), 1012.1343.
- [33] W. Lima, G. Matsas, and D. Vanzella, *Phys. Rev. Lett.* **105**, 151102 (2010), 1009.1771.
- [34] P. Jetzer, *Phys. Rep.* **220**, 163 (1992).
- [35] S. L. Liebling and C. Palenzuela (2012), 1202.5809.
- [36] D. J. Kaup, *Phys. Rev.* **172**, 1331 (1968).
- [37] R. Ruffini and S. Bonazzola, *Phys. Rev.* **187**, 1767 (1969).
- [38] M. Colpi, S. L. Shapiro, and I. Wasserman, *Phys. Rev. Lett.* **57**, 2485 (1986).
- [39] E. W. Mielke and F. E. Schunck, *Nucl. Phys.* **B564**, 185 (2000), gr-qc/0001061.
- [40] T. D. Lee, *Phys. Rev.* **D35**, 3637 (1987).
- [41] R. Friedberg, T. D. Lee, and Y. Pang, *Phys. Rev.* **D35**, 3640 (1987).
- [42] D. F. Torres, *Phys. Rev.* **D56**, 3478 (1997), gr-qc/9704006.
- [43] G. L. Comer and H. Shinkai, *Class. Quantum Grav.* **15**, 669 (1998), gr-qc/9708071.
- [44] D. F. Torres, A. R. Liddle, and F. E. Schunck, *Phys. Rev. D* **57**, 4821 (1998), gr-qc/9710048.
- [45] D. F. Torres, A. R. Liddle, and F. E. Schunck, *Class. Quantum Grav.* **15**, 3701 (1998), gr-qc/9803094.
- [46] M. Horbatsch and C. Burgess, *JCAP* **1108**, 027 (2011), 1006.4411.
- [47] R. V. Wagoner, *Phys. Rev. D* **1**, 3209 (1970), URL <http://link.aps.org/doi/10.1103/PhysRevD.1.3209>.
- [48] T. Harada, T. Chiba, K.-i. Nakao, and T. Nakamura, *Phys. Rev. D* **55**, 2024 (1997), URL <http://link.aps.org/doi/10.1103/PhysRevD.55.2024>.
- [49] M. Salgado (2002), gr-qc/0202082.
- [50] R. M. Wald, *General Relativity* (The University of Chicago Press, Chicago, U.S.A., 1984).
- [51] M. Alcubierre, *Introduction to 3+1 Numerical Relativity* (Oxford Univ. Press, New York, 2008), ISBN 978-0-19-920567-7.
- [52] M. Alcubierre and M. D. Mendez, *Gen. Rel. Grav.* **43**, 2769 (2011), 1010.4013.
- [53] C. Palenzuela, I. Olabarrieta, L. Lehner, and S. L. Liebling, *Phys. Rev.* **D75**, 064005 (2007), gr-qc/0612067.
- [54] C. Palenzuela, L. Lehner, and S. L. Liebling, *Phys. Rev.* **D77**, 044036 (2008), 0706.2435.
- [55] E. Seidel and W. Suen, *Phys. Rev.* **D42**, 384 (1990).
- [56] F. E. Schunck and E. W. Mielke, *Class. Quant. Grav.* **20**, R301 (2003), 0801.0307.
- [57] B. Bertotti, L. Iess, and P. Tortora, *Nature* **425**, 374 (2003).
- [58] J. Thornburg, *Phys. Rev.* **D59**, 104007 (1999), gr-qc/9801087.
- [59] T. Harada, T. Chiba, K.-i. Nakao, and T. Nakamura, *Phys. Rev.* **D55**, 2024 (1997), gr-qc/9611031.
- [60] M. Alcubierre and J. A. González, *Comp. Phys. Comm.* **167**, 76 (2005), gr-qc/0401113.
- [61] M. Ruiz, M. Alcubierre, and D. Nuñez, *Gen. Rel. Grav.* **40**, 159 (2008), 0706.0923.
- [62] M. Ruiz, D. Hilditch, and S. Bernuzzi, *Phys. Rev.* **D83**, 024025 (2011), 1010.0523.
- [63] Here and in what follows, Latin indices from the first part of the alphabet  $a, b, c, \dots$  will denote 4-dimensional quantities, while Latin indices from the middle of the alphabet

$i, j, k, \dots$  will denote 3-dimensional spatial quantities.